# Electro-optic sampling of high-speed devices and integrated circuits

by J. M. Wiesenfeld

The operating speeds of the fastest electronic devices and integrated circuits (ICs) have surpassed the capabilities of conventional electronic measurement instrumentation. Electro-optic sampling is an optical probing technique which has ultrashort temporal resolution and is capable of noninvasively probing ICs at internal nodes. This technique is voltage-sensitive because it relies upon the electric field produced by the signal voltage on the device under test (DUT). The electric field (and hence the voltage) can be sampled because it produces birefringence in an electrooptic crystal which changes the state of polarization of an ultrashort-duration optical probe pulse that propagates through the electrooptic crystal. The electro-optic crystal is the substrate of the DUT for direct probing, is a

<sup>©</sup>Copyright 1990 by International Business Machines Corporation. Copying in printed form for private use is permitted without payment of royalty provided that (1) each reproduction is done without alteration and (2) the *Journal* reference and IBM copyright notice are included on the first page. The title and abstract, but no other portions, of this paper may be copied or distributed royalty free without further permission by computer-based and other information-service systems. Permission to *republish* any other portion of this paper must be obtained from the Editor.

crystal on a separate test structure for hybrid probing, and is a separate crystal placed above the DUT for external probing. Temporal resolution below 1 ps and a sensitivity below 0.1 mV/ $\sqrt{\text{Hz}}$  have been demonstrated (though not in the same experiment). The principles of electro-optic sampling are reviewed in this paper. Selected applications for measurement of high-speed waveforms in discrete devices and in ICs are presented.

# 1. Introduction

The very high speeds at which electronic devices and integrated circuits (ICs) are now capable of operating have created a measurement problem. For example, selectively doped heterostructure transistors having 10-ps average propagation delay times at room temperature [1], as well as pseudomorphic InGaAs/InAlAs modulation-doped field-effect transistors (MODFETs) with an extrapolated  $f_{\rm MAX}$  of 200 GHz [2], have been fabricated. Also, digital ICs with a clock frequency above 26 GHz have been reported [3]. To evaluate such devices, measurement techniques that provide both high temporal resolution and the ability to probe noninvasively at internal points of the IC are required. Conventional

electronic test methods are either too limited in bandwidth or too invasive at high frequencies to characterize such devices successfully.

A variety of new testing techniques, some of which are discussed in this journal issue, have been demonstrated to overcome these difficulties. This paper describes one of these new techniques, electro-optic sampling, which is an optical probing technique [4]. The physical basis of this probing technique is the electro-optic effect, in which the presence of an electric field across an appropriate substrate induces a field-dependent birefringence in the substrate. The birefringence affects an optical probe beam by altering its state of polarization. If the field is caused by a voltage on the device, the change of polarization of the probe beam can be related directly to the voltage. Thus, electro-optic sampling is a voltage-sensitive technique. When the optical probe beam is a train of ultrashort (picosecond-duration) pulses, very-high-speed voltage waveforms can be resolved, because the pulses act as sampling gates. The technique is applicable to internal probing of ICs, because the optical probe is spatially localized and can be focused to  $\sim 1-\mu m$  diameter. There is no mechanical contact between the device under test (DUT) and the probe, so if the substrate is transparent at the wavelength of the probe beam, electro-optic sampling is noninvasive.

Electro-optic sampling requires a substrate that exhibits a linear electro-optic effect. Materials which have an inversion center of symmetry, such as silicon, necessarily do not exhibit a linear electro-optic effect, and cannot be probed by electro-optic sampling. Three basic variations of electro-optic sampling may be distinguished, depending upon the relationship between the substrate in which the electro-optic effect is observed and the DUT: direct, external, and hybrid sampling. In direct electrooptic sampling, the DUT is fabricated on a substrate that is itself electro-optic, and the probe beam senses the fields produced by voltages in the DUT via the electro-optic effect in the substrate. Direct electro-optic sampling has been applied to devices fabricated on GaAs and InP substrates. For external and hybrid sampling, the DUT need not be fabricated on an electro-optic substrate, so measurements can be performed on silicon, as well as GaAs or InP, devices. In external sampling, a crystal of an electro-optic material, such as LiTaO3 or GaAs, is placed above the DUT, so that the electric fields from the DUT penetrate into the sampling crystal. In hybrid sampling, a discrete sampler, which is usually composed of a microstrip transmission line deposited on an electrooptic material, is electrically connected to the DUT, so that voltage waveforms produced in the DUT are coupled into the sampler. In both external and hybrid sampling, the probe beam does not propagate through the DUT, but rather through the sampling crystal.

The use of the electro-optic effect to measure high-speed electrical signals was first demonstrated by Auston and co-workers [5, 6]. The technique was extended to higher sampling rates [7] and finer temporal resolution and voltage sensitivity [4] by subsequent workers. The first applications of electro-optic sampling to the measurement of waveforms internal to integrated circuits were reported in 1985 [8, 9]. There have been several recent reviews on the topic of electro-optic sampling [10–17]. The reader is referred to these reviews for greater detail in various aspects of the technique than that presented here.

This paper is organized as follows. Section 2 describes the basic physics of the electro-optic effect and its specific application to the measurement of signals from high-speed devices. Technical aspects of the implementation of electro-optic sampling for measuring high-speed repetitive waveforms are presented in Section 3. Illustrative applications are presented in Section 4. The results given there are not a complete account of the body of work that has by now been published. For more extensive references, the reader is again referred to the reviews cited above. Finally, some limitations and future directions for electro-optic sampling are discussed in Section 5.

# 2. Principles of the electro-optic effect

The description of the electro-optic effect begins with the definition of the impermeability tensor of a crystal,  $\eta$ , whose elements are given (in MKS units) by

$$\eta_{ij} = \frac{\epsilon_0}{\epsilon_{ij}} = \frac{1}{n_{ii}^2},\tag{1}$$

where  $\epsilon_{ij}$  is an element of the dielectric tensor for the crystal,  $\epsilon_0$  is the permittivity of vacuum, and  $n_{ij}$  is an element of the refractive index tensor of the crystal. The propagation of light through the crystal is described in terms of the index ellipsoid, which is given by

$$\eta_{ii} x_i x_i = 1, \tag{2}$$

where  $x_i$ , i=1, 2, or 3, is a Cartesian coordinate. In Equation (2) and henceforward, the convention of summation over repeated indices is assumed. In the principal coordinate system, the dielectric tensor is diagonal,  $n_{ij}=n_i\delta_{ij}$ , and the index ellipsoid is also diagonal. The ellipsoid surface in coordinate space described by Equation (2) can be used to determine the index of refraction for a light wave propagating with wave vector **k** through the crystal. The major and minor axes of the ellipse formed by the intersection of the index ellipsoid with the plane normal to **k** define the orientation and magnitude of the ordinary and extraordinary indices of refraction for the light wave. For a particular polarization **D** of the light wave, the index of

refraction is given by the magnitude of this ellipse along the direction **D**.

The electro-optic effect is described in terms of the electric field dependence of the impermeability tensor [18]:

$$\eta_{ii}(\mathbf{E}) = n_{ii}(0) + r_{iik}E_k + s_{iikl}E_kE_l + \cdots$$
 (3)

E is a low-frequency (below optical frequency) electric field imposed on the crystal. The coefficients  $r_{ijk}$  are the linear or Pockels electro-optic coefficients, and the coefficients  $s_{ijkl}$  are the quadratic or Kerr electro-optic coefficients. The linear electro-optic coefficients vanish because of symmetry considerations for crystals with inversion symmetry, such as silicon. The weaker quadratic electro-optic effect is present in all materials. For the remainder of this paper we consider only the linear electro-optic effect.

It can be shown from symmetry considerations that the indices i and j (and k and l) in Equation (3) can be permuted [18]. To take advantage of this permutation symmetry, we introduce contracted indices as follows:  $(ij) \rightarrow k$ ;  $(11) \rightarrow 1$ ,  $(22) \rightarrow 2$ ,  $(33) \rightarrow 3$ ,  $(23) = (32) \rightarrow 4$ ,  $(13) = (31) \rightarrow 5$ , and  $(12) = (21) \rightarrow 6$ . With contracted indices, Equation (3) becomes

$$\eta_i(\mathbf{E}) = \eta_i(0) + r_{ik}E_k,\tag{4}$$

where i = 1-6 and k = 1-3. In the principal coordinate system in which  $\epsilon_{ij}$  is diagonal, Equations (1) and (4) are combined to give

$$\left[\frac{1}{n_1^2} + r_{1k}E_k\right]x^2 + \left[\frac{1}{n_2^2} + r_{2k}E_k\right]y^2 + \left[\frac{1}{n_3^2} + r_{3k}E_k\right]z^2 + 2yzr_{4k}E_k + 2xzr_{5k}E_k + 2xyr_{6k}E_k = 1.$$
 (5)

The electro-optic tensor has up to 18 independent elements  $r_{ik}$ , but this number is further reduced by crystal symmetry. **Table 1** gives the form of the electro-optic tensors for two crystal symmetries important for electro-optic sampling experiments: cubic  $\overline{4}3m$  (for example, GaAs and InP) and trigonal 3m (for example, LiNbO<sub>3</sub> and LiTaO<sub>3</sub>) [19].

We next consider specific examples. Figure 1 shows the cross sections of two crystals with electrodes applied in microstrip configuration. The application of a voltage V on the top electrode produces an electric field in the z direction of magnitude  $E_z = V/L$  or V/d in Figures 1(a) and 1(b), respectively. In Figure 1(a), the light travels essentially parallel to the direction of the electric field; in Figure 1(b) the light travels perpendicular to the field direction. The manifestations of the electro-optic effect are therefore referred to as *longitudinal* and *transverse* for Figures 1(a) and 1(b), respectively.

First we consider the longitudinal electro-optic effect, which is appropriate for crystals of  $\overline{43}m$  symmetry. For

Table 1 Electro-optic tensors.

	43 <i>m</i> (GaAs, InP, etc.)	
0 0 0 r <sub>41</sub> 0 0	0 0 0 0 r <sub>4</sub> 1	0 0 0 0 0 0 r <sub>41</sub>
	3 <i>m</i>	
	(LiNbO <sub>3</sub> , LiTaO <sub>3</sub> , etc.)	
$\begin{bmatrix} 0 \\ 0 \\ 0 \\ 0 \\ -r_{51} \\ -r_{22} \end{bmatrix}$	$-r_{22}$ $r_{22}$ $0$ $r_{51}$ $0$ $0$	r <sub>13</sub> r <sub>33</sub> 0 0 0

such crystals the principal axes are the (100) crystallographic directions, and in the absence of an applied electric field the crystals are isotropic with index of refraction n. From Table 1 and Equation (5), the index ellipsoid in the presence of the field  $E_{-}$  is

$$\frac{x^2}{n^2} + \frac{y^2}{n^2} + \frac{z^2}{n^2} + 2r_{41}xyE_z = 1.$$
 (6)

The last term on the left-hand side of Equation (6) mixes the x and y axes. The new principal axes for the index ellipsoid are x', y', and z, where

$$\hat{\mathbf{x}}' = \frac{1}{\sqrt{2}} (\hat{\mathbf{x}} + \hat{\mathbf{y}}),$$

$$\hat{\mathbf{y}}' = \frac{1}{\sqrt{2}} \left( -\hat{\mathbf{x}} + \hat{\mathbf{y}} \right).$$

The index ellipsoid becomes

$$\left[\frac{1}{n^2} + r_{41}E_z\right]{x'}^2 + \left[\frac{1}{n^2} - r_{41}E_z\right]{y'}^2 + \frac{z^2}{n^2} = 1.$$
 (7)

The indices of refraction along the new principal axes are

$$n_{x'} = n - \frac{1}{2} n^3 r_{41} E_z,$$

 $n_{r} = n$ 

$$n_{y'} = n + \frac{1}{2} n^3 r_{41} E_z \,,$$

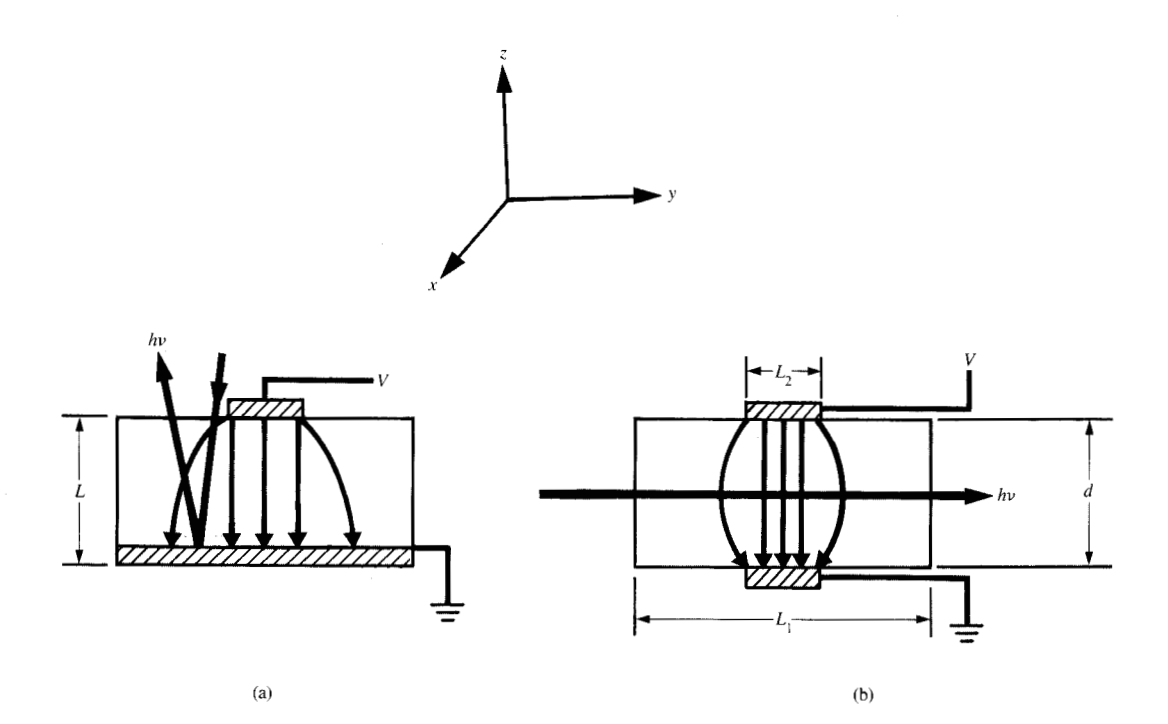
crystal to become birefringent and has created new

where we have assumed that 
$$n^2 r_{41} E_z \ll 1$$
. Thus, the application of an electric field along  $\hat{\mathbf{z}}$  has caused the  $\overline{4}3m$ 

45111

143

(8)



Cross sections of microstrip transmission lines on electro-optic crystals. (a) Geometry for longitudinal electro-optic effect. (b) Geometry for transverse electro-optic effect.

principal axes in the x-y plane rotated by 45° from the (100) and (010) axes.

Because the crystal has become birefringent, it can function as a wave plate. It is therefore possible to construct a modulator based on the electro-optic effect, as shown in **Figure 2**. The electric field is produced by the applied voltage and is oriented parallel to z. Let the input optical wave be polarized along x, as shown. The difference in phase accumulated by the y' and x' components of the input optical wave is the retardation  $\Gamma$ , given by

$$\Gamma = \frac{2\pi (n_{y'} - n_{x'})L}{\lambda} = \frac{2\pi n^3 r_{41} V}{\lambda},$$
(9)

where Equation (8) has been used and  $\lambda$  is the vacuum wavelength of the optical wave. For the moment, neglect the static quarter-wave ( $\lambda/4$ ) retardation plate in Figure 2. Then, the optical intensity passed through the output polarizer,  $I_T$ , which is crossed to the input polarizer, is

$$I_{\rm T} = I_0 \sin^2 \left(\frac{\Gamma}{2}\right),\tag{10}$$

where  $I_0$  is the intensity incident on the input polarizer. A graph of Equation (10), which is the transfer function for the electro-optic modulator of Figure 2, is shown in **Figure 3**. When  $\Gamma = \pi$ , the transmission of the modulator is unity. The voltage applied to the modulator which produces this half-wave retardation is the half-wave voltage,  $V_-$ , which is, from Equation (9),

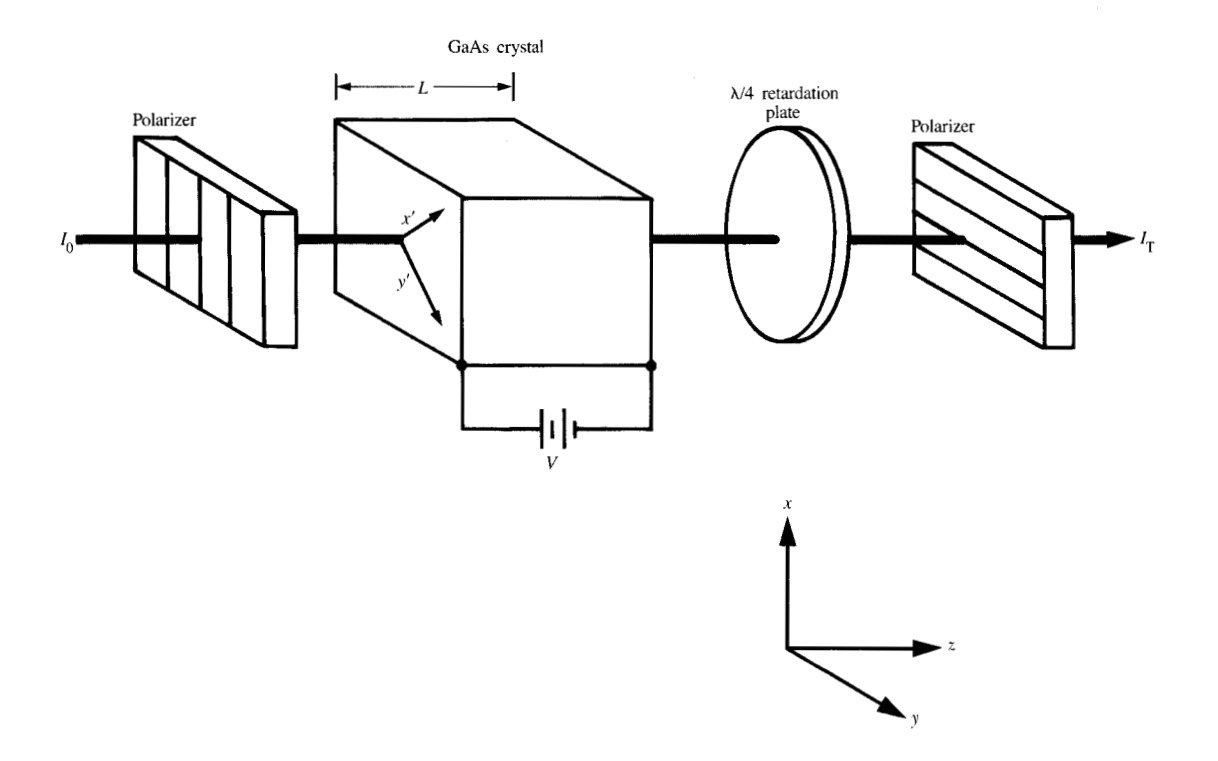
$$V_{\pi} = \frac{\lambda}{2n^3 r_{41}}. (11)$$

In terms of  $V_{\pi}$ , Equation (10) can be written

$$I_{\rm T} = I_0 \sin^2(\pi V / 2V_{\pi}). \tag{12}$$

For GaAs,  $r_{41} = 1.2 \times 10^{-12}$  m/V and n = 3.60 at  $\lambda = 1.0 \, \mu \text{m}$  [19], so  $V_{\pi} = 8.9$  kV. For circuit applications, voltages across the GaAs substrate are about 1 V, so the retardation and fractional transmission changes caused by this voltage are  $\sim 10^{-4}$ .

To maximize the sensitivity and linearity of the modulator in Figure 3 for small applied voltages (relative to  $V_{\pi}$ ), it is necessary to maximize  $dI_{\rm T}/d\Gamma$  or, equivalently,  $dI_{\rm T}/dV$ . For the transfer function of



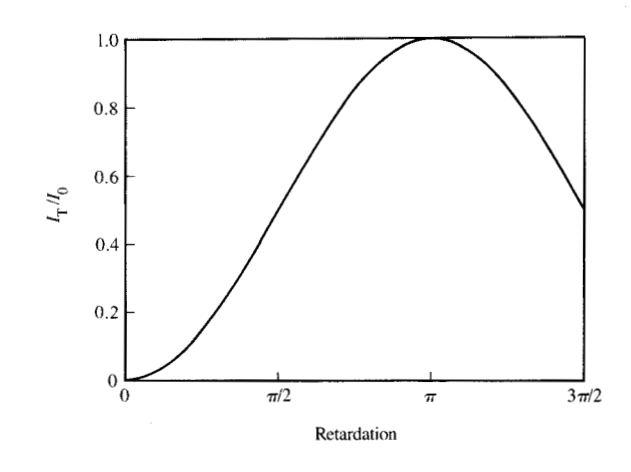
Intensity modulator based on the electro-optic effect. A voltage V is applied along the z axis of a GaAs crystal of length L. Principal axes of the induced birefringence, x' and y', as well as the principal axes (100) of the unperturbed crystal are shown.

Equation (10), this occurs at  $\Gamma_0 = \pi/2$ . The value of  $\Gamma$  to be used in Equation (10) is the total retardation caused by all optical components placed between the crossed polarizers in Figure 3; it therefore includes the static  $\lambda/4$  wave plate. This wave plate causes the optical wave to become circularly polarized and optically biases the modulator to a value of  $\Gamma_0 = \pi/2$ . If we allow the possibility that the retardation of the static wave plate deviates from  $\pi/2$  by a small angle  $\delta$ , the total retardation between the crossed polarizers in Figure 3 is  $\Gamma = \pi/2 + \delta + \pi V/V_{\pi}$ . Using Equation (10) and some trigonometric identities gives

$$I_{\rm T} = I_0/2 \left[ 1 + \sin \left( \pi V/V_{\pi} + \delta \right) \right].$$
 (13)

The fractional modulation is  $\Delta I/I = [I_{\rm T}(V) - I_{\rm T}(0)]/I_{\rm T}(0)$ , where  $I_{\rm T}(V)$  and  $I_{\rm T}(0)$  are the transmission through the analyzer when voltage V and no voltage, respectively, are applied to the modulator. Because  $\pi V/V_{\pi} \ll 1$ , a series expansion is performed on Equation (13) to obtain

$$\frac{\Delta I}{I} = \frac{\pi V}{V_{\pi}} - \frac{\delta}{2} \left(\frac{\pi V}{V_{\pi}}\right)^2 - \frac{1}{6} \left(\frac{\pi V}{V_{\pi}}\right)^3 + \cdots$$
 (14)



## Flatine 6

Transfer function for the modulator of Figure 2

For a signal of  $\sim 1 V$  and  $\delta \sim 1^{\circ}$ , the second and third terms on the right-hand side of Equation (14) are  $\sim 10^{-6}$  and  $\sim 10^{-8}$  times the first term on the right-hand side. Indeed, at the quarter-wave bias point, the range of linearity of the electro-optic effect, as expressed by the spurious free dynamic range, can exceed 100 dB [12].

We now consider the transverse electro-optic effect, as illustrated in Figure 1(b). The 3m crystals LiNbO<sub>3</sub> and LiTaO<sub>3</sub> have a natural (that is, field-independent) birefringence, with the c axis parallel to the z axis. The index ellipsoid for a 3m crystal with the electric field applied along the z axis is, from Equation (5) and Table 1,

$$\left(\frac{1}{n_o^2} + r_{13}E_z\right)x^2 + \left(\frac{1}{n_o^2} + r_{13}E_z\right)y^2 + \left(\frac{1}{n_e^2} + r_{33}E_z\right)z^2 = 1,$$
(15)

where  $n_0$  and  $n_e$  are the ordinary and extraordinary indices of refraction, and x and y are the principal axes orthogonal to the c axis. The principal axes are unchanged by the field, but the indices of refraction are modified as follows:

$$n_{x} = n_{o} - \frac{1}{2} n_{o}^{3} r_{13} E_{z},$$

$$n_{y} = n_{o} - \frac{1}{2} n_{o}^{3} r_{13} E_{z},$$

$$n_{z} = n_{e} - \frac{1}{2} n_{e}^{3} r_{33} E_{z}.$$
(16)

For an optical beam propagating along the y axis, as shown in Figure 1(b), with input polarization at 45° to the x and z axes, the retardation, apart from the static wave plate, is

$$\Gamma = \frac{2\pi}{\lambda} (n_e - n_o) L_1 - \frac{\pi}{\lambda} (n_e^3 r_{33} - n_o^3 r_{13}) \frac{L_2}{d} V,$$
 (17)

where  $L_1$  and  $L_2$  are the widths of the crystal and the region of the electric field (approximately the width of the electrodes), respectively, d is the thickness of the crystal, and  $V=E_zd$ . The first term in Equation (17) is the retardation caused by the static birefringence of the crystal, and the second term is the birefringence caused by the electro-optic effect. The static retardation can be removed or converted to a bias  $\Gamma_0=\pi/2$  using a compensator [4]. The electro-optic half-wave voltage derives from the second term and is

$$V_{\pi} = \frac{\lambda d}{L_2 (n_{\rm e}^3 r_{33} - n_{\rm o}^3 r_{13})}.$$
 (18)

For the 3m crystal,  $V_{\pi}$  depends on the geometry of the

crystal, because of the factor  $d/L_2$ . For LiTaO<sub>3</sub> at the wavelength 1.2  $\mu$ m,  $r_{13} = 6.2 \times 10^{-12}$  m/V,  $r_{33} = 26.7 \times 10^{-12}$  m/V,  $n_o = 2.1305$ , and  $n_e = 2.1341$  [19]. Therefore,  $V_\pi = 6.0 d/L_2$  kV. For an electrode configuration on the LiTaO<sub>3</sub> crystal corresponding to a 50- $\Omega$  transmission line,  $V_\pi \approx 50$  kV. Modulation by the electro-optic effect in 3m crystals obeys Equations (12)–(14), with  $V_\pi$  given by Equation (18).

# 3. Technical aspects

# Sampling geometries

The most important geometries for electro-optic sampling are shown in **Figure 4**. Figures 4(a)-4(c) show probing geometries using the longitudinal electro-optic effect; Figures 4(d) and 4(e) show geometries using the transverse electro-optic effect. Geometries 4(a), 4(b), and 4(e) are useful for probing planar ICs, 4(c) is useful for probing an IC in microstrip configuration, and 4(d) is the geometry necessary for a hybrid sampler using a 3m electro-optic crystal.

The arrangement shown in Figure 4(a) is the back-side probing geometry for coplanar ICs made on substrates of GaAs or InP  $(\overline{4}3m \text{ symmetry})$ . The probe beam enters from the rear of the substrate, reflects off the electrode at which the waveform to be sampled appears, and exits through the rear surface. The spatial resolution is determined by the size of the focused near-infrared probe beam, which can be as small as  $\sim 1 \mu m$  in diameter. For optimum performance, the back surface of the IC should be smooth and the electrode should be a good reflector of the probe beam, which, in fact, metallic contacts are. The retardation experienced by the probe beam is twice that given by Equation (9), because the probe beam passes through the substrate twice. The voltage V in Equation (9) is the difference in potentials between the electrode and the rear surface.

Front-side probing geometries relevant to GaAs or InP ICs with coplanar or microstrip configurations are shown in Figures 4(b) and 4(c), respectively. In both configurations, the probe beam enters from the front or top side of the IC, which must be of good optical quality, reflects off the back surface, and exits from the front surface. As in the back-side probing geometry, the retardation accumulated by the probe beam is twice that given by Equation (9). Note, however, that the potential difference V to be used is the difference in potentials between the front and rear surfaces at the positions where the beam enters and reflects, and is not the same as the difference between the contact and the rear surface. Because the potential on the front surface decreases as the distance from the electrode being probed increases, the retardation is smaller than in the back-side probing geometry [16]. An alternative way of viewing the same

tront-side probing than for back-side probing.

the reduced sensitivity and spatial resolution of the front-

front-side geometry in most cases. However, in spite of

Accordingly, the back-side geometry is preferable to the

the back surface, so the spot size at the front surface is, at

the front-side probing geometry, the beam is focused on

modulation is smaller than in the back-side geometry. In

field is weaker than that directly under the contact. Thus,

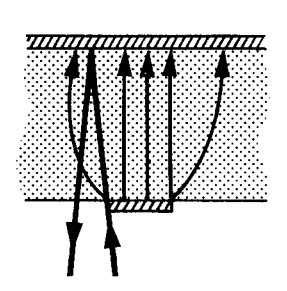
of the electrode, where the longitudinal component of the 4(b) and 4(c) propagates through the fringing electric field

to back-side probing because the probe beam in Figures

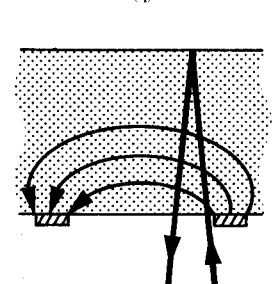
phenomenon is that the retardation is reduced compared

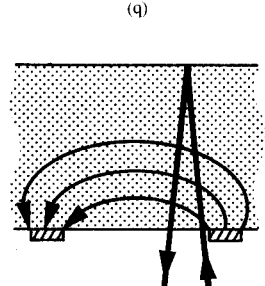
beam [16]. Thus, the spatial resolution is poorer for best, \$\langle\$ times larger than the size of the focused probe

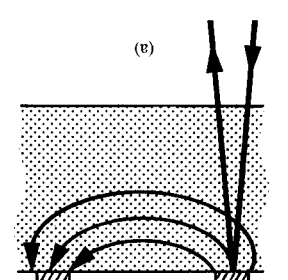
in the front-side probing geometry the electro-optic

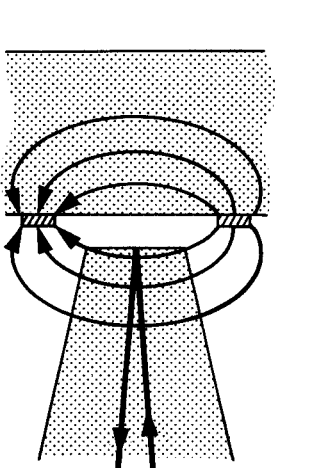


(5)

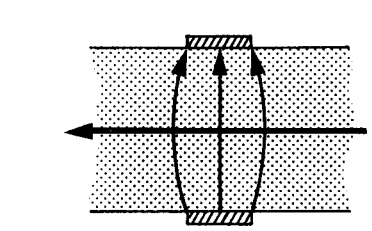








(a)



(p)

transverse electro-optic effect. side probing for a microstrip geometry. (d) Transverse probing for a microstrip geometry. (e) External probing of a coplanar device using the Probing geometries for electro-optic sampling. (a) Back-side probing for a coplanar device. (b) Front-side probing for a coplanar device. (c) Front-

is impossible to implement. packaged ICs [21] for which cases the back-side geometry can be used to effectively analyze microstrip [8, 20] or side probing geometry compared to back-side probing, it

respect to the electrical waveform propagating on the the probe beam is directed at the proper angle with the position at which the probe traverses the crystal. If potential difference between top and bottom surfaces at the retardation is given by Equation (17), where V is the The probe beam enters one side and exits the other, so 4(d) is used for hybrid samplers made from 3m materials. optic effect, respectively. The geometry shown in Figure 4(c) and 4(d) for the longitudinal and transverse electrotransmission lines, with geometries as shown in Figures Hybrid samplers have been fabricated as microstrip

transmission line, it is possible to match the optical velocity with the electrical velocity and reduce transit time limitations to the temporal resolution of electro-optic sampling [4]. Such velocity matching is not possible for cubic crystals.

Figure 4(e) shows the geometry appropriate for external electro-optic sampling of a signal on a coplanar IC using a crystal of 3m symmetry [22]. No electrodes are applied to the sampling crystal. The field inside the crystal is the field in the half-plane above the DUT. As shown, the probing optical beam is incident from the top and reflects off the bottom surface of the sampling crystal, which may be coated for high reflectivity. The retardation accumulated by the probe beam is twice that given in Equation (17), because the probe makes two passes through the field. The appropriate V in Equation (17) is the difference in potentials from one side of the sampling crystal to the other. How this relates to the difference in potential between the two electrodes depends on the detailed geometry of the DUT and sampling crystal and also on the dielectric constant of the sampling crystal. This scheme for electro-optic sampling is promising. because it can be used with devices fabricated on silicon (which is not itself electro-optic) as well as GaAs or InP. However, spatial resolution may be limited because the maximum transverse electro-optic effect occurs when the probe beam is placed between the two electrodes; in complicated circuit geometries this may lead to interference or crosstalk between voltages propagating on different lines. This effect might be reduced by using an external prober fabricated in a material exhibiting the longitudinal electro-optic effect, in which the external sampler could be placed directly over the electrode where the signal is to be probed [17]. In addition, the effect of capacitive loading, caused by proximity of a highdielectric material, on the operation of the IC under study needs to be explored more carefully.

Geometries 4(b), 4(c), and 4(e) can be applied to measurement of any devices, including packaged devices. The back-side probing geometry 4(a) requires access to the back surface of the IC and so is not applicable to probing a packaged device. However, geometries 4(a), 4(b), 4(c), and 4(e) can be implemented for wafer probing. Indeed, wafer probe stations modified for optical access have been developed using geometries 4(a) [15] and 4(e) [17].

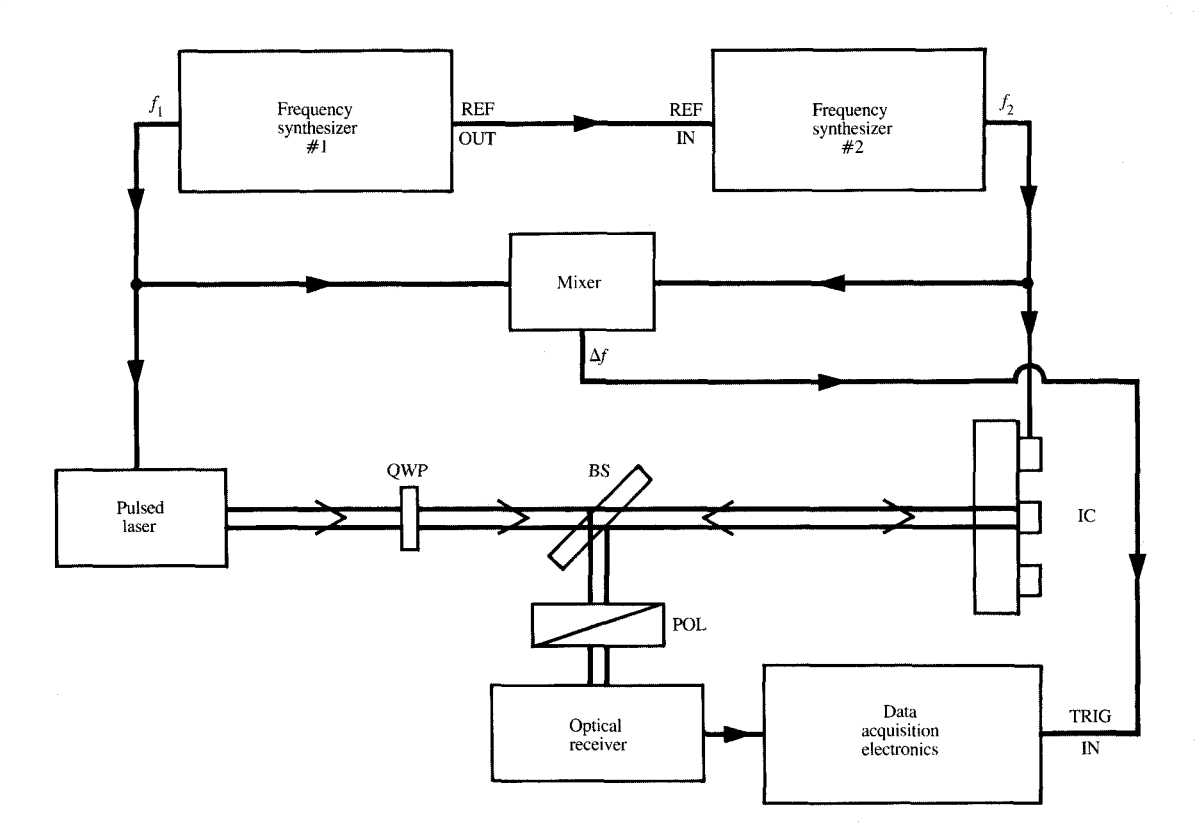
# • Experimental system arrangements

Regardless of the exact probing geometry used, a generalized experimental schematic for electro-optic sampling can be described. Distinctions are made between electronic and optical excitation of the DUT, and between measurement in the time and frequency domains.

A generalized schematic for measurement of waveforms internal to an IC (by direct electro-optic sampling) using electrical excitation is shown in Figure 5. Two frequency synthesizers are phase-locked together and generate signals at frequencies  $f_1$  and  $f_2$ , which drive a pulsed laser and the IC, respectively. The probe beam is biased to  $\Gamma_0 = \pi/2$  by passage through a quarter-wave plate (OWP) and is focused onto the DUT. The probe beam interrogates the DUT from the back side, as in geometry 4(a), is reflected by the contact to a beamsplitter, and is directed through a polarizer into a receiver. With obvious modifications, the other geometries in Figure 4 can be used with the same optical arrangement. (When the probing is performed with a crystal of 3m symmetry, the optical bias is achieved with a compensator rather than with the quarter-wave plate, as discussed previously.) The nearly circular polarization of the probe beam is deformed into elliptical polarization via the electro-optic effect caused by the voltage on the contact being probed, and this is converted into an amplitude change by the analyzer. The frequencies of the synthesizers are set so that  $f_2$  is equal to an integral multiple of  $f_1$  plus a small offset,  $\Delta f$ . Successive pulses from the probe laser therefore sweep across the waveform at the rate  $\Delta f$ , which is the sampling rate. The sampling rate can vary from 10 Hz to 100 kHz, depending on the particular experiment. A microwave mixer generates a signal at  $\Delta f$  which is used to trigger the data acquisition electronics.

When the data acquisition electronics consists of a time-domain device such as an oscilloscope or a signal averager, a replica of the sampled waveform is reconstructed at the rate  $\Delta f$ . The frequency response of the DUT at the point being probed can be measured directly when the data acquisition electronics consists of a frequency-domain device, such as a spectrum analyzer, vector voltmeter, or lock-in amplifier [15, 20, 23]. The basis for the frequency-domain measurement can be understood by noting that in the frequency domain the electro-optic effect can be viewed as a mixer [11], which produces sum and difference frequency components between the drive frequency of the device  $f_2$  and the pulse repetition rate of the laser  $f_1$ . The difference frequency  $\Delta f$ is readily isolated from the other frequencies by the frequency-domain data acquisition electronics. Measurement of the power and phase at  $\Delta f$  as the frequency  $f_2$  is varied gives the frequency response of the DUT directly.

The DUT can also be excited optically. Figure 6 shows a schematic for hybrid electro-optic sampling of the impulse response of a photodetector which has been illuminated with an optical pulse [24]. Pulses from a mode-locked laser are divided into two beams. One beam provides excitation of the photodetector; the other is the

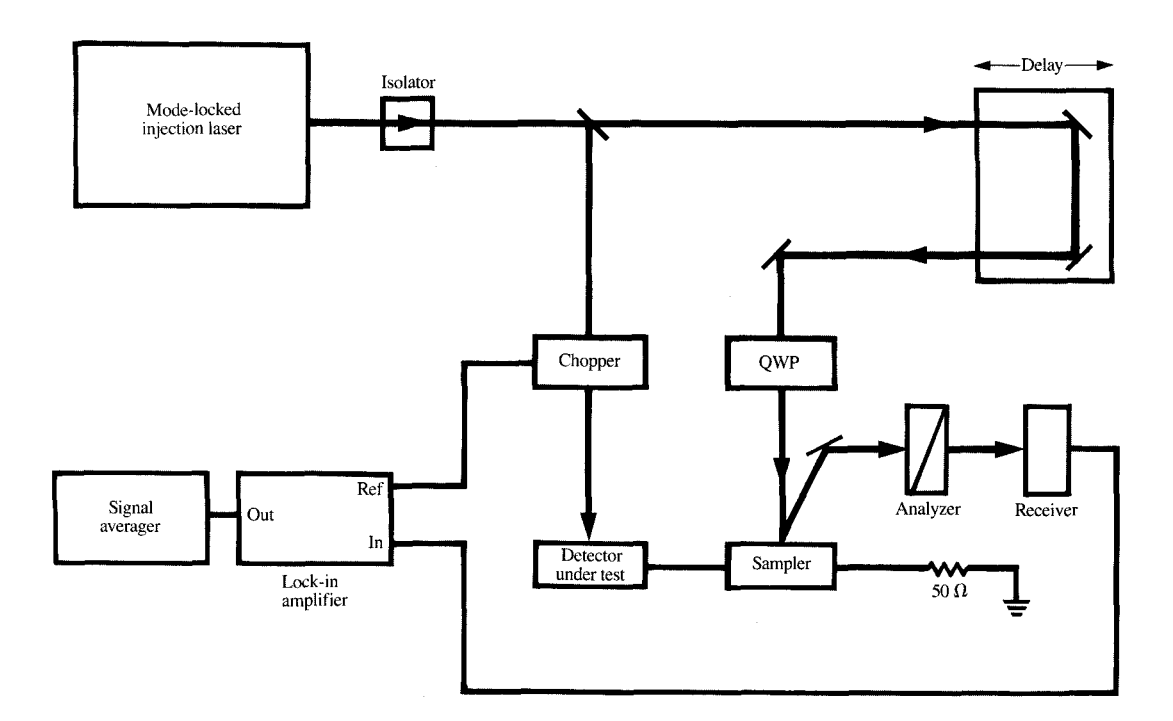


## Emma E

General experimental schematic for electro-optic sampling with electrical excitation of the DUT. QWP, BS, and POL are quarter-wave plate, beamsplitter, and polarizer, respectively.

probe beam. The excitation pulse produces a voltage pulse in the photodetector, which is coupled to a hybrid sampler fabricated in microstrip geometry on GaAs [Figure 4(c)]. The probe beam is biased by the quarterwave plate, focused onto the back surface of the hybrid sampler, reflected from this surface, and directed through an analyzer into a receiver. The temporal waveform is reconstructed by varying the delay between the voltage pulse traveling on the hybrid sampler and the probe pulse by using a mechanical delay line, as shown in Figure 6. For optical excitation and probing of ICs, the detector and sampler are considered to be combined, and a photoactive element of the IC, such as a GaAS MESFET, is illuminated [25]. In this case, the optical pulse causes a change in logic state of the photoactive element, which can produce waveforms of complex shape at other places in the IC that depend on the particular operation of the IC.

The laser source must operate at a wavelength at which the electro-optic substrate is transparent. Thus, for direct and hybrid sampling of GaAs or InP, two types of lasers have been used: pulse-compressed mode-locked Nd:YAG lasers operating at 1.06  $\mu$ m [11, 25], and gain-switched or mode-locked InGaAsP diode lasers operating at 1.3 μm or 1.55  $\mu$ m [26, 27]. The Nd:YAG laser source produces pulses of 1-3-ps duration at a repetition rate near 100 MHz, and with greater than 100 mW of usable average power [15]. The considerably more compact injection laser sources produce pulses of 10-20-ps duration at repetition rates up to 20 GHz, with average power of about 1 mW. For electrical excitation of a DUT at gigahertz frequencies, the drive to the DUT is synchronized to a high harmonic (>10) of the repetition rate of the Nd:YAG laser and to the fundamental of the injection laser. Mode-locked visible dye lasers, with subpicosecond pulse duration, ~50 mW average power,



Schematic for electro-optic sampling with optical excitation of the DUT. Specific details are shown for hybrid sampling of a photodiode DUT.

and 100-MHz repetition rate, have been used for hybrid and external probing with LiNbO<sub>3</sub> and LiTaO<sub>3</sub> samplers. Some of the trade-offs involved in using the various laser sources are described in forthcoming sections.

## • Temporal resolution

The effects which contribute to the temporal resolution of the electro-optic sampling measurement are the intrinsic response time of the electro-optic effect, transit time effects, the laser pulse duration, and timing jitter between the excitation signal and the probe pulse. The retardation experienced by the probe beam will be that caused by the electrical signal averaged over the applicable times. Because the electro-optic effect is an electronic optical nonlinearity, its intrinsic response time will be in the subpicosecond range and will be negligible compared to other effects.

The two relevant transit times are the electrical and optical transit times [11, 15]. The electrical transit time is the propagation time of the electrical signal across the diameter of the optical probe beam. For a probe beam radius of 3  $\mu$ m on a GaAs substrate, the electrical transit time will be 40 fs, which is again negligible compared to

other effects [16]. The optical transit time is a more significant limitation to the temporal resolution, especially for direct probing of GaAs or InP. The optical transit time is the propagation time of the optical pulse through the region of electric field within the electro-optic material. Assuming that the field has a large amplitude throughout the substrate, as, for example, in a microstrip transmission line [Figure 1(a)], an upper limit for the optical transit time  $\Delta t_{\rm OTT}$  is given by

$$\Delta t_{\rm OTT} = \frac{2nL}{c} \,. \tag{19}$$

For a 250- $\mu$ m-thick GaAs substrate (n=3.5),  $\Delta t_{\rm OTT}=5.8$  ps. For coplanar structures, the geometry of the contacts can confine the electric field to a region much smaller than the thickness of the substrate, causing a reduction in the appropriate L in Equation (19) and, therefore, a reduction in  $\Delta T_{\rm OTT}$ . The optical transit time can also be reduced by matching the velocity of the electrical signal with a component of the velocity of the optical beam, which is possible for the transverse geometry in LiTaO<sub>3</sub> or LiNbO<sub>3</sub> samplers [4], but is not possible for GaAs or InP [11].

150

The probe pulse duration can be a major limitation on the temporal resolution, depending on the laser used. This is particularly true when semiconductor diode lasers are used, because their 10–20-ps pulse durations will usually be larger than transit times. For direct sampling experiments, the 1–3-ps duration pulse from the Nd:YAG laser source may be smaller than the optical transit time effect. The highest-temporal-resolution experiments have been achieved using subpicosecond pulses from a visible mode-locked dye laser with a hybrid LiTaO, sampler [10].

Timing jitter is caused by random fluctuations of the probe pulse repetition period with respect to the period of the electrical signal on the DUT. It is thus related to the phase noise of the probe laser pulse train. Timing jitter has been measured for Nd:YAG lasers [28], mode-locked and gain-switched InGaAsP diode lasers [29], synchronously mode-locked dye lasers [30], and passively mode-locked dye lasers [31]. For the mode-locked Nd:YAG laser source, the timing jitter is 2-11 ps, but this can be reduced to 0.3 ps by the application of a carefully designed external electrical feedback circuit [28]. The timing jitter in the pulsed InGaAsP diode lasers is less than 1 ps [29] and is therefore negligible compared to the pulse duration. Timing jitter in the synchronously mode-locked dye laser was measured to be  $\sim 20$  ps [30], but this type of laser has not been used in electro-optic sampling experiments. For the passively mode-locked dye laser (CPM laser), the relevant timing litter was  $\sim 2$  ps [31]. Presumably the jitter in the dye laser pulse trains could be reduced by using an external feedback circuit. However, timing jitter does not cause a problem in experiments using optical excitation when the excitation and probe pulses are derived from the same laser.

The overall temporal resolution is the convolution of all of the above effects. The most important effects are the optical transit time, the pulsewidth  $\Delta t_{\rm p}$ , and the timing jitter  $\Delta t_{\rm J}$ . As an estimate, a simple sum of squares (Gaussian) convolution form can be used to arrive at the overall temporal resolution  $\Delta t$ :

$$\Delta t = (\Delta t_{\rm OTT}^2 + \Delta t_{\rm P}^2 \Delta t_{\rm J}^2)^{1/2}.$$
 (20)

Note that the temporal resolution considered thus far gives the limitation for resolving a transition time of an electrical signal. It is possible, however, to measure propagation times for a pulse or other well-defined waveform to better accuracy, if no significant dispersion of the waveform occurs [32]. In this case, the limitation on temporal resolution is imposed by signal-to-noise considerations.

## • Sensitivity

Three important noise sources in the electro-optic sampling experiment are shot noise in the detected probe

beam, thermal noise in the photoreceiver, and excess laser noise (that is, noise in the probe beam in excess of shot noise). Neglecting the excess laser noise and assuming that  $V \ll V_{\pi}$ , the signal-to-noise ratio S/N of the measured electro-optic signal is [11, 16]

$$S/N = \frac{i_{\text{avg}}^2 \left(\frac{\pi V_0}{2 V_{\pi}}\right)^2 R_{\text{L}}}{4 q i_{\text{avg}} R_{\text{L}} B + 8 k T B},$$
(21)

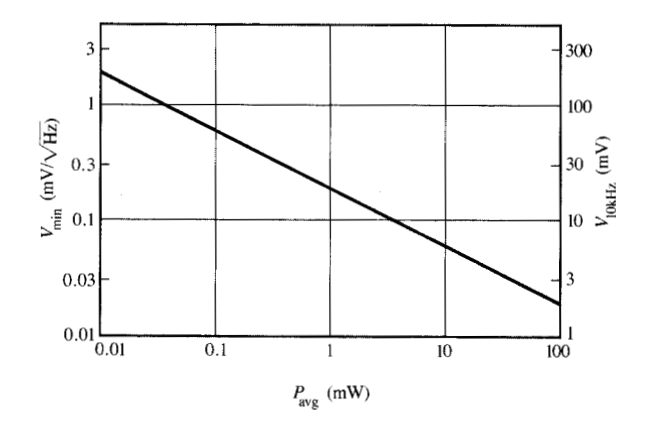
where  $i_{\text{avg}}$  is the average photocurrent at the receiver,  $V_0$  is the peak amplitude of the electrical signal,  $R_{\text{L}}$  is the load resistor on the photodetector, q is the electron charge, B is the bandwidth of the data acquisition electronics, k is Boltzmann's constant, and T is the temperature. In writing Equation (21), bias at the quarter-wave point and a signal waveform that is positive only have been assumed. The best sensitivity (highest S/N) is achieved in the shot-noise limit, where the first term in the denominator of Equation (21) is much larger than the second term. The minimum detectable voltage  $V_{\min}$  is defined to be the voltage that produces a signal-to-noise ratio of unity in a 1-Hz detection bandwidth [11]. In the shot-noise limit, this is given by

$$V_{\min} = \frac{4V_{\pi}}{\pi} \sqrt{q/RP_{\text{avg}}}, \qquad (22)$$

where R is the responsivity (in amperes per watt) of the photodetector,  $P_{\text{avg}}$  is the average optical power incident on the receiver, and  $i_{\text{avg}} = RP_{\text{avg}}$ . More extensive calculations of signal-to-noise ratio, including the effects of varying the optical bias  $\Gamma_0$  and the load resistor  $R_{\text{L}}$ , have been reported by Kolner and Bloom [11]. The factor of 4 in Equation (22) is a result of choosing a signal which is always positive; a factor of 2 is obtained for a sinusoidal signal. Thus, there is a small ambiguity in the defining equation for  $V_{\text{min}}$ .

Equation (22) gives a theoretical sensitivity that has not been attained in practice. Figure 7 shows a graph of  $V_{\rm min}$  as a function of received optical power  $P_{\rm avg}$ . Also shown is the signal voltage that will produce a signal-tonoise ratio of unity when the detection bandwidth is 10 kHz. Obviously, the more probe power available, the higher is the sensitivity. Thus, higher sensitivity can be achieved with the more powerful mode-locked Nd:YAG probe laser source than with the semiconductor probe laser sources. With an electro-optic sampling system based on a Nd:YAG probe laser, several mW of probe power is detected and a sensitivity of 70  $\mu V/\sqrt{Hz}$ , which is a factor of two from the shot-noise limit, has been achieved [15]. With an electro-optic sampling system based on a semiconductor diode laser, about 50 µW of power is incident on the receiver, and the sensitivity is about 1.5 mV/ $\sqrt{\text{Hz}}$ , which is also a factor of two from





## E GILLEY

Shot-noise-limited sensitivity as a function of average optical power incident on the receiver.  $V_{\rm 10kHz}$  is the voltage necessary to produce a signal-to-noise ratio of unity when the bandwidth of the electronic detection system is 10 kHz.

the shot-noise limit [14, 26]. Electro-optic sampling using a dye laser and the external prober has achieved a sensitivity of several mV/ $\sqrt{\text{Hz}}$  [22], which is further from the shot-noise limit.

It is clear from Equation (21) that the signal-to-noise ratio is enhanced by using the narrowest possible bandwidth B for the data acquisition electronics. One way to accomplish this is the use of signal-chopping techniques and subsequent data processing with phase-sensitive electronics [4, 11, 15]. By chopping at a high enough frequency, it is also possible to translate the frequency of data processing above the low frequencies where excess laser noise can be significant. Alternatively, the data can be collected in a narrow band around the offset frequency  $\Delta f$  [14, 26]. This works well for diode laser sources which have little excess laser noise.

The linearity of the measurement depends on the optical bias and the sensitivity, and has been discussed in detail by Kolner and Bloom [11, 12]. At the quarter-wave bias point and for an operating sensitivity of  $20 \ \mu V/\sqrt{Hz}$ , the electro-optic probe signal is linear to within a deviation of  $10^{-3}$  over a range of 140 dB.

## • Invasiveness

For direct probing experiments, but also in the hybrid sampling case, the creation of free carriers by absorption of the probe beam is a potential cause of invasiveness. The probe beam wavelength is chosen to be longer than the band edge of the substrate to minimize carrier

generation by direct band-to-band absorption. However, direct absorption by impurities and free carriers is possible. The further the probe wavelength from the band edge, the smaller is the absorption due to impurities. Thus, a probe wavelength of 1.3 µm is acceptable for GaAs substrates (band edge at 0.89  $\mu$ m), as is the 1.06μm wavelength produced by Nd:YAG lasers. For a GaAs substrate moderately doped to a level of  $1 \times 10^{17}$  cm<sup>-3</sup>, the free-carrier absorption at 1.3  $\mu$ m is 1% in a 200- $\mu$ m length [33], which may begin to be significant. Fortunately, many high-speed devices are fabricated on semi-insulating substrates, and the thickness of doped regions is very small. For an external sampler made from LiTaO<sub>3</sub>, which is used with a dye laser with a wavelength near 0.6  $\mu$ m, the absorption edge is near 0.3  $\mu$ m, so direct absorption and impurity absorption are not a problem.

Nonlinear optical effects should also be considered. Generation of free carriers by two-photon absorption becomes a problem when the probe beam becomes too intense. For GaAs, the two-photon absorption coefficient is  $\sim 20$  cm/GW at 1.06- $\mu$ m fundamental wavelength [34], so to avoid excessive carrier generation, the probe beam peak intensity should be limited below 100 MW/cm<sup>2</sup>. The inverse electro-optic effect will produce a dc voltage by optical rectification in electro-optic materials. For an intensity of 100 MW/cm<sup>2</sup>, this effect may produce about 50  $\mu$ V in a transmission-line structure on GaAs [16], which is small compared to signals to be measured and can also be discriminated against by phase-sensitive data-collection techniques.

Capacitive loading is a potential problem for the external probing scheme. Because the external crystal of LiTaO<sub>3</sub> has a large dielectric constant ( $\epsilon \sim 45$ ), it will disturb the electric field in the half plane above the IC being tested and may affect the operation of the DUT. Placement of a LiTaO<sub>3</sub> crystal above a coplanar waveguide transmission line on a silicon substrate has produced a propagation delay but no measurable distortion (on the  $\sim 1$ -ps time scale) for a short electrical pulse [17]. The possible effects of close placement of such a large-dielectric material in the vicinity of a transistor or other active device remain to be studied.

## • Crosstalk

The electro-optic modulation of the probe beam is proportional to the difference in potential between the front and back surfaces of the electro-optic substrate in both the longitudinal and transverse probing configurations. The potentials are due to the electric fields emanating from all contacts on the DUT, not just from the contact being probed. Thus, if the field from a nearby line is sufficiently strong at the spatial position of the probe beam, the signal from the nearby line will also be sampled by the probe beam. This leads to electro-optic

crosstalk, which may exist even when there is no electrical crosstalk on the device.

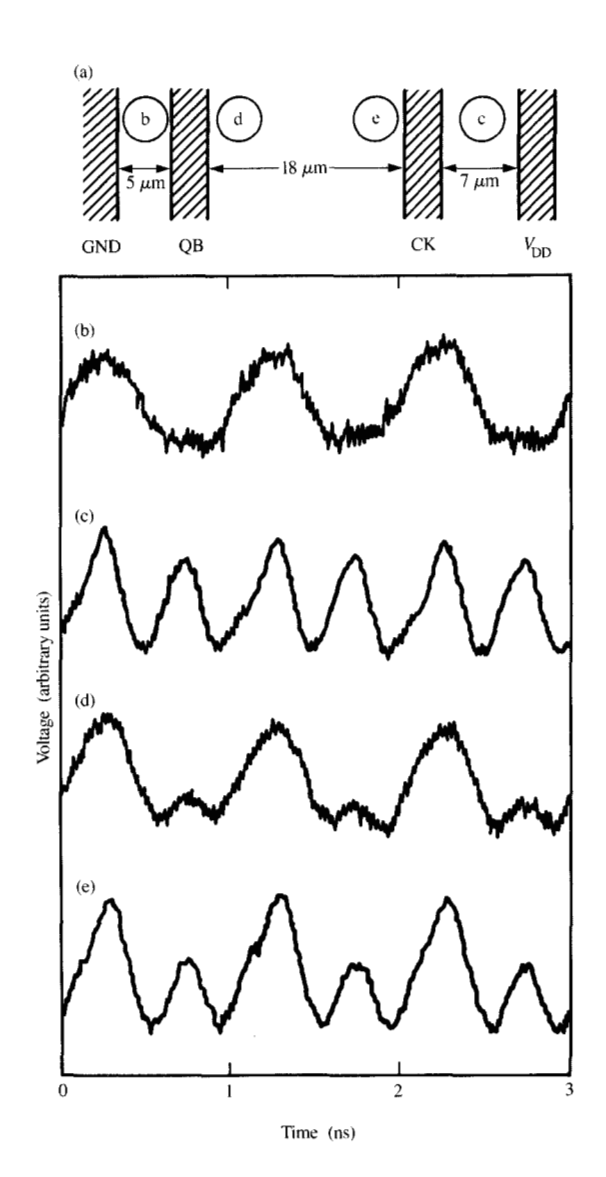
An example of electro-optic crosstalk is shown in Figure 8 [21]. Figure 8(a) shows the layout of a section of a GaAs IC with four contact lines: OB and CK are active signal and clock lines, respectively, and GND and  $V_{\rm DD}$ are ground and 2-V bias supply lines, respectively. The IC is packaged and therefore is probed from the front side [geometry 4(b)] at four positions, labeled b-e in Figure 8(a). The waveforms measured at these positions are shown by curves (b)-(e) in Figure 8. Curve (b) shows a 1-GHz sine wave, which represents a 101010 ... data stream at 2 GHz that is present on QB. Curve (c) shows a 2-GHz sine wave which is the clock signal on CK. For both curves (b) and (c), the probe beam is positioned between the active line being probed and an inactive (that is, constant-voltage) line. Curves (d) and (e) are obtained with the probe positioned between the two active lines, and the measured signals are a superposition of the signals carried by QB and CK, weighted more strongly by the closer line. Thus, curves (d) and (e) demonstrate electro-optic crosstalk. In the front-side probing geometry, crosstalk is reduced by probing between active and inactive lines, rather than between two active lines.

Crosstalk also arises in the back-side probing geometry [Figure 4(a)] because the back surface potential contains contributions from all (and especially the closest) signalcarrying lines on the front side [35]. Note that in the back-side probing geometry, the potential of the front surface at the probe position is well defined, because it is exactly the potential of the line being probed. The nonzero potential of the back surface is of the order of 10% or smaller than the potential of the front surface, when the substrate is thicker than the width of the electrode on the front surface [36], so the crosstalk is expected to be less than 10% of the signal. The nonzero potential of the back surface also affects the calibration from the measured electro-optic signal to the inferred voltage on the line being probed [36]. Establishment of a ground potential on the back surface may eliminate the crosstalk and calibration problems in back-side probing [13].

The external probing geometry [Figure 4(e)] should show crosstalk effects similar to those for the front-side probing geometry, since the external crystal (of 3m symmetry) must be placed between contacts on the front side of the DUT. Preferably, the crystal should be placed between the active line to be probed and an inactive line.

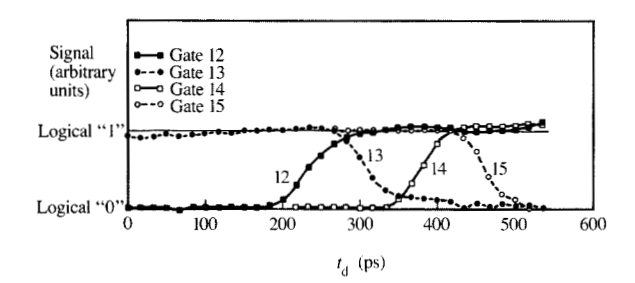
# 4. Results

In this section selected measurements of high-speed electrical signals obtained by electro-optic sampling are presented. The results are classified according to the

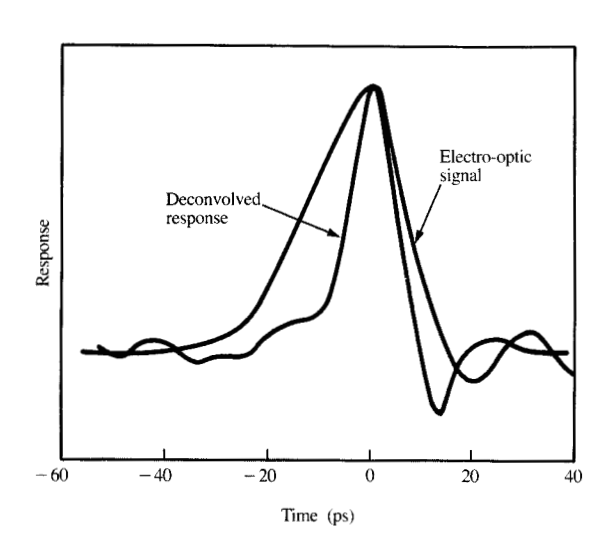


Measured crosstalk between active lines. (a) Layout of electrode configuration. (b), (c), (d), and (e) are waveforms measured by probing at positions indicated in (a). CK and QB have 2-GHz and 1-GHz signals, respectively, and GND and  $V_{\rm DD}$  are ground and 2-V bias lines, respectively. From [21], reproduced with permission; © 1988 IEEE.

excitation method and distinguished according to probing geometry. Results are presented for both analog and digital devices. The results are neither exhaustive nor in chronological order; rather, they are meant to be illustrative of the capabilities of the various embodiments of electro-optic sampling. More complete coverage of the



Waveforms produced by a switching transition of gate 10 in an inverter string. From [25], reproduced with permission.



Measured and deconvolved impulse response for a back-illuminated InGaAs/InP punch-through photodiode. From [41], reproduced with permission.

variety of experiments performed with electro-optic sampling can be found in other reviews [15–17].

## Optical excitation

One early and continuing application involves detection of very short electrical pulses and level transitions generated by photoconductive switches, using hybrid or external probing. For these studies, a subpicosecond mode-locked dye laser was chosen to ensure the best temporal resolution. The earliest demonstrations of electro-optic sampling involved optical excitation of a photoconductive switch followed by hybrid sampling using a LiNbO<sub>3</sub> sampler [4]. Subsequently, using a coplanar waveguide structure on a hybrid LiTaO3 sampler and subpicosecond pulses from a mode-locked dye laser, the rise time of a different photoconductor was measured to be 0.46 ps, demonstrating that subpicosecond resolution was attainable [37]. To study the dispersive characteristics of various electrical waveguide transmission lines, pulse shapes derived from photoconductive switches were measured at various positions along transmission lines on normal [17] and superconducting substrates [17, 38], using an external sampler. Recently, the shape of an electrical pulse 0.56 ps in duration (FWHM) produced by subpicosecond optical excitation of a CdTe-on-sapphire photoconductor has been resolved using external electro-optic sampling [39]. The measured rise time was 0.49 ps and the deconvolved pulse duration (FWHM) was 0.48 ps.

Optical excitation and direct probing have been used to analyze on-chip waveforms and propagation delays in a GaAs test IC, which consisted of a string of 20 inverter gates [25]. In that work, the logic state of a gate in the string was changed by optical excitation, from the front side of the IC, of an appropriate FET in the gate, using frequency-doubled pulses from a mode-locked Nd:YAG laser (2 ps, 532 nm, 6 pJ). Waveforms from subsequent gates in the string were measured by direct probing of the GaAs IC from the back side, using pulses at the fundamental wavelength from the same laser. Figure 9 shows data resulting when gate 10 was optically switched from logical "0" to logical "1". From the measurement of the transitions of downstream gates, such as those of gates 12-15, which are shown in Figure 9, the propagation delays of individual gates are determined. From the measurements [25], the propagation delays range from 72 to 78 ps, with ~3-ps uncertainty. Note that timing jitter is not a problem in the optical excitation experiment, because the excitation pulse (532) nm in this experiment) and the probe pulse (1064 nm in this experiment) derive from the same initial laser pulse.

An example of the use of optical excitation combined with hybrid electro-optic sampling is the measurement of the impulse response of very-high-speed photodiodes [24, 40, 41]. The experimental arrangement for this measurement has been shown in Figure 6. In the experiment of Wang and Bloom [40], the photodiode was bonded directly to the microstrip transmission line on the hybrid sampler, which was fabricated as a balanced microstrip line on a LiTaO<sub>3</sub> substrate. The photodiode was excited and the sampler was probed with picosecond pulses from a mode-locked dye laser. Note that the duration of the laser pulse enters the measured signal

twice, and so can be deconvolved from the data as the autocorrelation of the laser pulse, which can be measured accurately and independently of the electro-optic sampling measurement. The measured -3-dB bandwidth of the GaAs Schottky photodiode was 100 GHz, corresponding to an impulse response (FWHM) of 5.4 ps [40].

For optical communications applications, InGaAs photodiodes, which are responsive at 1.3 µm and 1.55  $\mu$ m, are important. The impulse response of the fastest long-wavelength InGaAs p-i-n photodiode has been measured using hybrid electro-optic sampling [41]. The device studied was a back-illuminated InGaAs/InP punch-through p-i-n with an active area of 150  $\mu$ m<sup>2</sup> and an intrinsic layer thickness of 0.5  $\mu$ m [42]. The photodiode was mounted in a low-inductance package and bonded directly to the center pin of a K connector [42]. The photodiode package was connected directly to a hybrid sampler, which consisted of a 50- $\Omega$  microstrip transmission line on a GaAs substrate, which was in turn connected to the bias T for the photodiode. Thus, the response could be measured free of the parasitics of the bias T. Excitation and probe pulses were derived from a mode-locked 1.3-µm InGaAsP external-cavity semiconductor laser, which produced pulses of ~11-ps duration. The measured electro-optic response of the photodiode and its deconvolved impulse response are shown in Figure 10. The width (FWHM) of the impulse response is less than 9 ps. The deconvolved frequency response is shown in Figure 11. There are ripples of magnitude 2 dB, and the -3-dB bandwidth is 67 GHz. From a circuit analysis of the mount used in these measurements, it appears that parasitic inductance and capacitance limit the bandwidth [41].

# • Electrical excitation

Most of the application of electro-optic sampling to the investigation of ICs has involved direct sampling of electrically driven GaAs-based ICs. The first results for direct probing of GaAs ICs were reported in 1985 for analog [8] and digital [9] ICs. In the many subsequent studies, waveforms at internal nodes, propagation delays of individual FETs or logic gates, and the direct frequency-domain response at various internal nodes have been reported for both digital and analog ICs. Some highlights are presented below.

The highest-clock-frequency digital IC studied by electro-optic sampling has been an 18-GHz static frequency divider [43]. The frequency dividers [44] were implemented by either capacitively enhanced logic (CEL) or buffered FET logic (BFL), and were fabricated with 0.2- $\mu$ m-gate-length MESFETs. This divider circuit contains a biphase clock master-slave D-flip-flop design, with the  $\overline{O}$  output of the slave fed back to the D input of

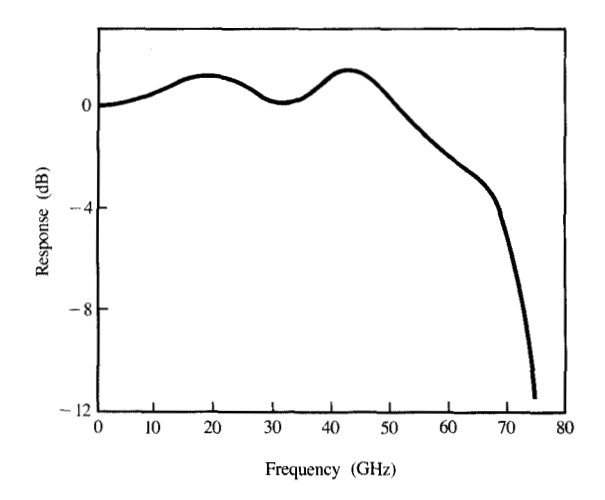
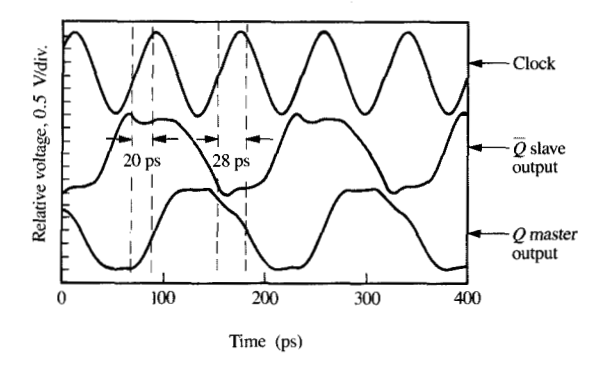


## FIGURE S

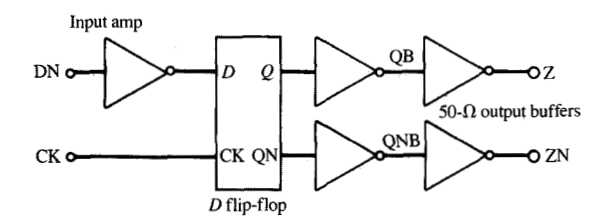
Frequency response determined for InGaAs/InP photodiode. Bandwidth (-3 dB) is 67 GHz. From [41], reproduced with permission.



## Floring I

Waveforms measured internal to CEL divider circuit operating at 12.1 GHz. From [43], reproduced with permission.

the master. The IC was sampled using a mode-locked, pulse-compressed Nd:YAG laser and an on-wafer probing station [15]. Sampled waveforms from the CEL divider, operating at 12.1 GHz, are shown in Figure 12. The waveforms shown are the clock, the  $\overline{Q}$  output of the slave, and the Q output of the master. The critical delay that determines the maximum toggle frequency of the



Block diagram of GaAs MESFET decision circuit (AT&T 494A) From [21], reproduced with permission; © 1988 IEEE.

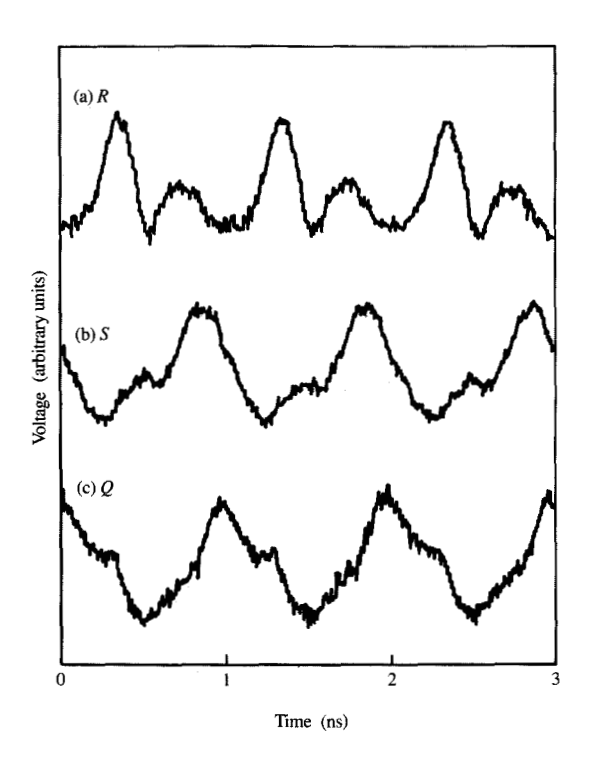


# Figure 14

Waveforms measured internal to R/S flip-flop in decision circuit. From [21], reproduced with permission; © 1988 IEEE.

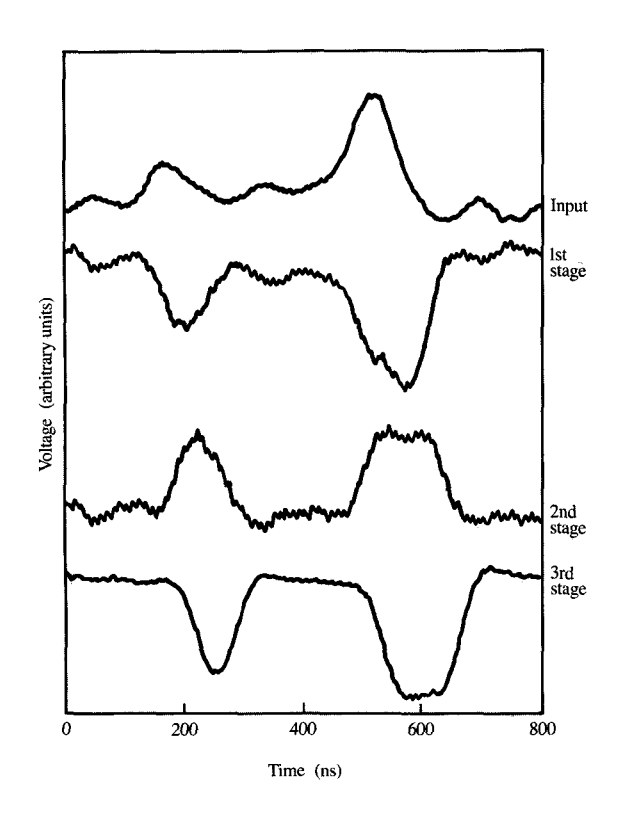
flip-flop is the longer of the two delays between the rising edge (50% point) of the clock and the rising or falling edge of the master Q waveforms. These delays are 20 ps and 28 ps, respectively, as shown in Figure 12. Thus, the maximum toggle frequency is predicted to be  $(2\tau_a)^{-1}$ ,

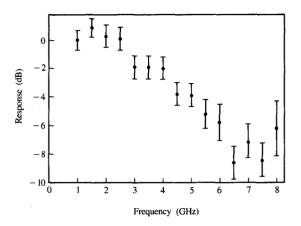
where  $\tau_{\rm d}$  is the critical delay, which corresponds to 17.9 GHz. Conventional electronic measurements on this IC suggest a maximum toggle frequency of 17.8 GHz, in good agreement with the results obtained by electro-optic sampling.

A detailed analysis was performed of a packaged planar GaAs decision circuit, whose function is to amplify data with respect to a logic threshold and to synchronize it to a reference clock signal [21]. The circuit was fabricated using GaAs enhancement/depletion-mode n-channel MESFET technology. The circuit was probed using pulses from a gain-switched InGaAsP laser (~22-ps duration) synchronized to electronic excitation of clock and data input signals. Because the device is packaged, the front-side probing geometry was used. A schematic of the decision circuit is shown in Figure 13. Data are amplified in the input amplifier, which contains three FETs, and synchronized to the clock in the D flip-flop. The circuit was evaluated with a 2-GHz clock frequency, and the data input was a 1-GHz sine wave (simulating a 1010 · · · data pattern); the laser was driven at 1 GHz minus a 1-kHz offset. Waveforms in an R/S flip-flop, which is internal to the D flip-flop, are shown in Figure 14. When the reset (R) pulse is high, the flip-flop output (O) switches low; when the set pulse (S) is high, O switches high. The set and reset pulses are synchronized to the clock, so Q has a fixed phase with respect to the clock. The non-idealities in the waveforms are apparent. Nevertheless, the output pulse derived from Q is properly square in shape [21]. Propagation delays in each of the three FETs in the input amplifier were measured by applying pulses from a comb generator to the data input at a 1-GHz rate; results are shown in Figure 15. The comb generator produced two pulses, the second of which saturated in the amplifier. The measured propagation delays for the three amplifiers were  $29 \pm 5$ ,  $18 \pm 2$ , and  $29 \pm 3$  ps, for stages 1 to 3, respectively. The response of the first FET has also been measured directly in the frequency domain, using a microwave spectrum analyzer in place of a signal averager for the data acquisition electronics [23]. The measured response, which has a -3-dB frequency of 4 to 4.5 GHz, is shown in Figure 16.

High-speed analog ICs have also been studied using electro-optic sampling. The signal propagation, frequency response, and distortion characteristics of GaAs MMIC multistage traveling-wave amplifiers (TWAs) have been characterized using direct probing and a Nd:YAG laser-based system [20]. For these experiments, frequency-domain measurements were performed to determine the small-signal frequency response, and time-domain measurements were performed to measure waveform distortion. The small-signal transfer function measured at the gate for stages 2–5 of a five-stage microstrip TWA is

156





## Home (a

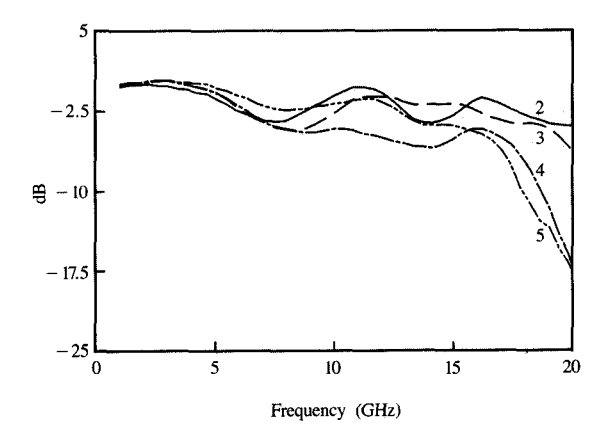
Small-signal measurement of frequency response of the first FET amplifier in the input amplifier section of the decision circuit. Bandwidth (-3 dB) is 4-4.5 GHz. From [23], reproduced with permission.

# Figure 15

Measurement of propagation delays in input amplifier section of decision circuit. Input waveform and waveforms after propagation through each of three FETs are shown. From [21], reproduced with permission; © 1988 IEEE.

shown in Figure 17. The measured responses were fitted to simulations, resulting in accurate evaluation of the circuit parameters [20]. From measurement of the small-signal response of the drains at each gate and from the distortion of large signals, propagation and interference between forward- and backward-traveling waves were observed. Electro-optic sampling techniques clearly facilitated the evaluation of these TWAs.

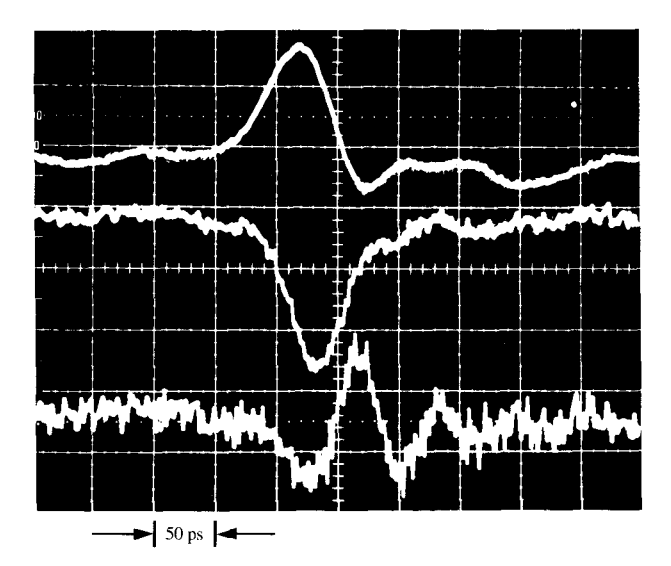
The temporal resolution afforded by electro-optic sampling has recently been dramatically tested by measurement of shock waves produced on nonlinear transmission lines fabricated on GaAs [45]. The nonlinear transmission line converts a 10-GHz sinusoidal input to an asymmetric waveform with a very fast fall time. By directly probing the device with a Nd:YAG-based electro-optic sampling system, the fall time of the shock wave was measured to be 2.5 ps. The system resolution was ~1.9 ps, so the fall time of the electrical shock wave was deduced to be 1.6 ps.



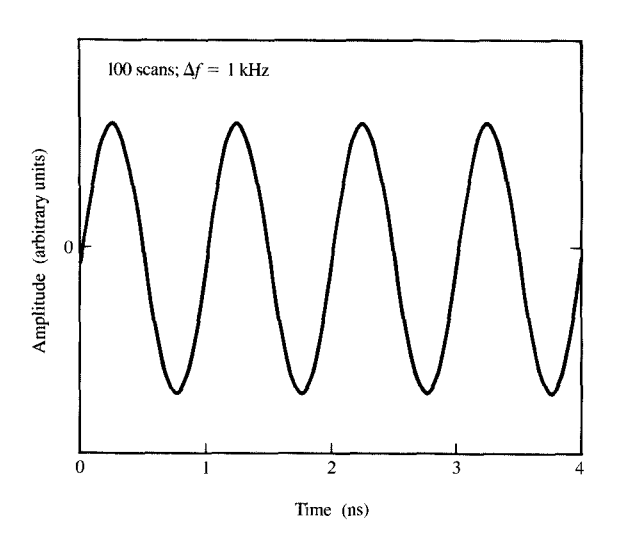
## Foure 17

Small-signal frequency response for successive gates in a five-stage distributed TWA. Devices are numbered in order of propagation for the forward wave. From [20], reproduced with permission; © 1986 IEEE.

Thus far, the examples presented have used direct probing of GaAs ICs. An InP-based IC has been analyzed using a gain-switched InGaAsP laser diode probe [32]. The circuit was a two-stage InGaAs/InP MESFET inverter, with the output of the first FET connected to



Propagation delays in a two-stage InGaAs/InP MESFET inverter circuit. From top to bottom, traces are input pulse from comb generator measured at the gate of the first FET, output of first FET, and output of second FET. From [32], reproduced with permission.



## Branzag

Waveform of 1-GHz clock signal internal to silicon NMOS 12-bit multiplexer circuit, measured by external electro-optic sampling. Courtesy of J. A. Valdmanis, Ultrafast Science Laboratory, University of Michigan, Ann Arbor, MI.

the gate of the second FET. Propagation delays, measured by driving the gate of the first FET with a pulse from a comb generator, are shown in Figure 18. The propagation delays of the first and second FETs were  $15 \pm 4$  ps and  $33 \pm 4$  ps, respectively. The electro-optic probe works as well in this InP-based IC as in GaAs ICs because the electro-optic  $r_{41}$  coefficient of InP [46] is equal, to within 10%, to that of GaAs.

Direct probing geometries have been much more widely applied to electrically excited DUTs because such DUTs have been ICs, predominantly fabricated on GaAs substrates. Hybrid probing has been applied to measure fast-output waveforms from small packaged devices such as comb generators [26, 27].

External probing has recently been used to evaluate internal waveforms in a GaAs selectively doped heterostructure transistor (SDHT) prescaler circuit [47] and in a 1.7-Gbit silicon NMOS 12-bit multiplexer circuit [17]. The external prober was fabricated of LiTaO<sub>3</sub>, and subpicosecond pulses from a mode-locked dye laser were used for the probe pulses [22]. The GaAs SDHT circuit was driven by electrical pulses produced by a fast photodiode excited by pulses from the dye laser, which were coupled to the input of the circuit. Waveforms were measured at various internal nodes in the prescaler circuit, and propagation delays were deduced. Crosstalk and circuit loading were also observed in the measurement [17]. The silicon multiplexer circuit was driven by an input sinusoid synchronized to the tenth harmonic of the ~100-MHz repetition rate of the passively mode-locked dye laser. Synchronization was achieved by converting an electrical pulse train, generated by a photodiode monitoring the dye laser pulse train, into a sinusoid which then served as a reference frequency for a synthesizer that drove the circuit. The timing jitter in this arrangement was  $\sim 2$  ps [31]. The 1-GHz clock signal measured internally in the silicon NMOS multiplexer is shown in Figure 19 [17]. Although many aspects of external electro-optic probing must be clarified, it is capable of measuring waveforms internal to silicon ICs, as the results of Figure 19 demonstrate.

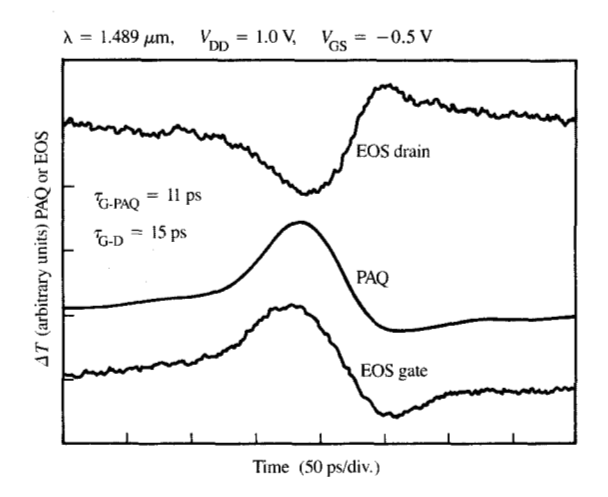
# Combination of electro-optic sampling with chargedensity probing

Optical probing techniques that are sensitive to freecarrier densities in active devices, as opposed to voltage, have been demonstrated [48, 49], but are less well developed than electro-optic sampling. However, such techniques can yield information complementary to that obtained by electro-optic sampling. Two recent experiments in which a charge-density probing technique has been used in combination with electro-optic sampling are described below.

Voltage and charge-density measurements were made optically on a reverse-biased GaAs Schottky diode using electro-optic sampling and an interferometric charge-

sensing technique, respectively [50]. The charge-sensing technique [48] relies on changes in the refractive index of the DUT that are caused by variations in free-carrier density internal to the DUT. Free carriers affect the refractive index via plasma, Burstein-Moss, and Franz-Keldysh effects [50, 51]. For silicon DUTs, the plasma effect is the dominant contribution, while for GaAs DUTs the plasma and Burstein-Moss effects are both significant. The free-carrier-induced changes in the refractive index are detected by interferometry: The probe beam is divided into two beams, one of which passes through the active region of the DUT in which the carrier density is varying; the other passes through an inactive region. The two beams are recombined after interrogating the DUT. Refractive index changes produce phase changes in one beam, which can be converted to intensity changes in the recombined probe beam by analyzing the polarization state of the recombined probe beam [48]. In this way, changes of carrier density can be determined. Keller et al. [50], using this charge-sensing technique, have measured the charge in a GaAs Schottky diode as a function of applied voltage. They have also measured the internal voltage across the Schottky diode as a function of applied voltage using electro-optic sampling. The combination of both techniques permits an internal measurement of the C-V characteristics of a DUT. They also observed a modulation of the measured charge-sensing signal with applied voltage from which the depth of the depletion layer in the device as a function of applied voltage could be determined.

The second charge-sensitive optical probing technique is phase-space absorption quenching (PAQ) [49]. PAQ is applicable to devices based on quantum-well (QW) structures, such as modulation-doped FETs (MODFETs). In this technique, the optical probe beam monitors changes in the absorption that occur in the QW in the gate channel when free carriers are present. Free carriers in the conduction band reduce the absorption by filling the upper states of the appropriate optical transitions. The fractional modulation of probe beam intensity can be as large as 2-4% for a device containing a single quantum well [49, 52]. The technique has been applied to measure carrier distributions in the gate channel as a function of voltage applied to an InGaAs/InAlAs MODFET [52, 53], and to measure high-speed (gigahertz-frequency) waveforms in the MODFET by probing in the gate channel [54]. Internal propagation delays were measured for the InGaAs/InAlAs MODFET by applying a short electrical pulse from a comb generator to the gate electrode, and measuring voltage waveforms under the gate and drain electrodes by electrooptic sampling (direct probing of the InP substrate) and charge density in the gate channel by PAQ sampling. The results of this measurement are shown in Figure 20 [54].



## Platitic 20

Internal propagation delay in InGaAs/InAlAs MODFET measured by a combination of electro-optic sampling (EOS) and phase-space absorption quenching (PAQ) sampling. From [54], reproduced with permission.

The delay between the voltage pulse on the gate electrode and the PAQ signal, which measures the appearance of charge in the channel, is 11 ps. The overall propagation delay from gate to drain is 15 ps. The 11-ps delay for the appearance of the PAQ signal represents the charging time for the channel. The combination of charge- and voltage-sensitive techniques used in this study [54] allows detailed investigation of the internal dynamics of veryhigh-speed devices using optical probing techniques only.

# 5. Concluding remarks

Electro-optic sampling is a voltage-sensitive probing technique capable of measuring electrical signals with a temporal resolution below 1 ps and noninvasively sampling waveforms internal to ICs. The demonstrated sensitivity is below 1 mV/ $\sqrt{\text{Hz}}$ . As shown by the examples presented above, electro-optic sampling has many embodiments and is therefore quite versatile. In particular, it has been applied to the evaluation of discrete devices, packaged ICs, and ICs in wafer form. For evaluating GaAs or InP ICs, direct sampling appears convenient and has been used successfully. Ultimately, the temporal response for direct sampling will be limited by the optical transit time effect, which, unless the substrate is specifically thinned, will be about 1-2 ps. For evaluation of silicon ICs, direct electro-optic sampling is impossible. External sampling may become a viable

technique for evaluation of silicon ICs, but needs further development. Most likely, a longitudinal electro-optic crystal will be used for external sampling to reduce potential crosstalk and calibration problems.

All techniques and measurements discussed in this paper involve some type of signal averaging of repetitive waveforms. This is necessary because the fractional modulation of the probe beam produced by ~1-V signals via the electro-optic effect is  $\sim 10^{-4}$ . It is desirable to probe the DUT as it is exercised with random or pseudorandom inputs. This will require real-time probing, which requires enhanced sensitivity. To achieve enhanced sensitivity, more probe power or a limitation on the bandwidth of the processing electronics is required. The latter option effectively means that for realtime probing, the DUTs must operate at lower-thangigahertz frequencies. To overcome this limitation, a realtime probing configuration, in which only selected instants of the waveform, rather than the entire waveform, are measured, might be possible. Alternatively, measurements of short-pattern repetitive waveforms can simulate the operation of the DUT with random data and will be sufficient for characterization.

Voltage calibration from the measured electro-optic signal is a topic that needs further investigation. The electro-optic signal will depend on the potential difference between front and back surfaces of the sampling substrate at the position of the probe beam. The exact potential distributions will have contributions from all contacts on the DUT and may require detailed modeling of the electric field to relate the electro-optic signal to the voltage at the test point. It will be important to develop "rules of thumb" that can convert general geometric features of the DUT into approximate calibration factors.

In spite of these difficulties, electro-optic sampling shows great promise as a high-speed measurement technique that can be used to characterize both discrete devices and ICs. It has already achieved notable success and has been used to evaluate a variety of devices. Electro-optic sampling can reasonably be expected to be of significant assistance in the ongoing development of electronic devices.

## References

- N. J. Shah, S. S. Pei, C. W. Tu, and R. C. Tiberio, "Gate Length Dependence of the Speed of SSI Circuits Using Submicrometer Selectively Doped Heterostructure Transistor Technology," *IEEE Trans. Electron Devices* ED-33, 543-547 (1986).
- T. Henderson, M. I. Aksun, C. K. Peng, H. Morkoc, P. C. Chao, P. M. Smith, K. H. G. Duh, and L. F. Lester, "Microwave Performance of Quarter-Micrometer Gate Low-Noise Pseudomorphic InGaAs/InAlAs Modulation-Doped Field Effect Transistor," *IEEE Electron Device Lett.* EDL-7, 649-651 (1986).
- U. K. Mishra, J. F. Jensen, A. S. Brown, M. A. Thompson, L. M. Jelloian, and R. S. Beaubien, "Ultra-High-Speed Digital Circuit Performance in 0.2-μm Gate-Length AlInAs/ GalnAs HEMT Technology," IEEE Electron Device Lett. EDL-9, 482-484 (1988).

- J. A. Valdmanis, G. Mourou, and C. W. Gabel, "Picosecond Electro-Optic Sampling System," *Appl. Phys. Lett.* 41, 211–212 (1982)
- D. H. Auston and A. M. Glass, "Optical Generation of Intense Picosecond Electrical Pulses," Appl. Phys. Lett. 20, 398–399 (1972).
- P. LeFur and D. H. Auston, "A Kilovolt Picosecond Optoelectronic Switch and Pockel's Cell," Appl. Phys. Lett. 28, 21–23 (1976).
- R. C. Alferness, N. P. Economou, and L. L. Buhl, "Picosecond Optical Sampling Technique for Measuring the Speed of Fast Electro-Optic Switch/Modulators," *Appl. Phys. Lett.* 37, 597–599 (1980).
- K. J. Weingarten, M. J. W. Rodwell, H. K. Heinrich, B. H. Kolner, and D. M. Bloom, "Direct Electro-Optic Sampling of GaAs Integrated Circuits," *Electron. Lett.* 21, 765-766 (1985).
- J. L. Freeman, S. K. Diamond, H. Fong, and D. M. Bloom, "Electro-Optic Sampling of Planar Digital GaAs Integrated Circuits," Appl. Phys. Lett. 47, 1083–1084 (1985).
- J. A. Valdmanis and G. A. Mourou, "Sub-Picosecond Electro-Optic Sampling: Principles and Applications," *IEEE J. Quantum Electron.* QE-22, 69-78 (1986).
- B. H. Kolner and D. M. Bloom, "Electrooptic Sampling in GaAs Integrated Circuits," *IEEE J. Quantum Electron.* QE-22, 79-93 (1986).
- B. H. Kolner, "Internal Electro-Optic Sampling in GaAs," Characterization of Very High Speed Semiconductor Devices and ICs, R. K. Jain, Ed., SPIE Proc. 795, 310–316 (1987).
- X. C. Zhang and R. K. Jain, "Analysis of High-Speed GaAs ICs with Electro-Optic Probes," *Characterization of Very High* Speed Semiconductor Devices and ICs, R. K. Jain, Ed., SPIE Proc. 795, 317–338 (1987).
- J. M. Wiesenfeld, A. J. Taylor, R. S. Tucker, G. Eisenstein, and C. A. Burrus, "Electro-Optic Sampling Using Injection Lasers," Characterization of Very High Speed Semiconductor Devices and ICs, R. K. Jain, Ed., SPIE Proc. 795, 339-344 (1987).
- K. J. Weingarten, M. J. W. Rodwell, and D. M. Bloom, "Picosecond Optical Sampling of GaAs Integrated Circuits," *IEEE J. Quantum Electron.* QE-24, 198–220 (1988).
- J. M. Wiesenfeld and R. K. Jain, "Direct Optical Probing of Integrated Circuits and High-Speed Devices," Measurements of High-Speed Signals in Solid State Devices, R. B. Marcus, Ed., in Semiconductors and Semimetals, R. K. Willardson and S. C. Beer, Eds., Vol. 28, Academic Press, Orlando, FL, 1990.
- J. A. Valdmanis, "Electro-Optic Measurement Techniques for Picosecond Materials, Devices, and Integrated Circuits," Measurements of High-Speed Signals in Solid State Devices, R. B. Marcus, Ed., in Semiconductors and Semimentals, R. K. Willardson and S. C. Beer, Eds., Vol. 28, Academic Press, Orlando, FL, 1990.
- A. Yariv and P. Yeh, Optical Waves in Crystals, John Wiley & Sons, Inc., New York, 1984.
- I. P. Kaminow, in CRC Handbook of Laser Science and Technology, M. J. Weber, Ed., Vol. IV, Part 2, CRC Press, Boca Raton, FL, 1986, pp. 253–278.
- M. J. W. Rodwell, M. Riaziat, K. J. Weingarten, B. A. Auld, and D. M. Bloom, "Internal Microwave Propagation and Distortion Characteristics of Traveling-Wave Amplifiers Studied by Electrooptic Sampling," *IEEE Trans. Microwave Theory Tech.* MTT-34, 1356–1362 (1986).
- M. S. Heutmaker, T. B. Cook, B. Bosacchi, J. M. Wiesenfeld, and R. S. Tucker, "Electro-Optic Sampling of a Packaged High-Speed GaAs Integrated Circuit," *IEEE J. Quantum Electron*. QE-24, 226-233 (1988).
- J. A. Valdmanis, "1-THz Bandwidth Prober for High-Speed Devices and Integrated Circuits," *Electron. Lett.* 23, 1308-1310 (1987).
- J. M. Wiesenfeld and M. S. Heutmaker, "Frequency Response of an Internal Amplifier in a High-Speed Integrated Circuit Measured by Electro-Optic Sampling," *Electron. Lett.* 24, 106-107 (1988).

- A. J. Taylor, J. M. Wiesenfeld, R. S. Tucker, G. Eisenstein, J. R. Talman, and U. Koren, "Measurement of a Very-High-Speed InGaAs Photodiode Using Electro-Optic Sampling," *Electron. Lett.* 22, 325-327 (1986).
- X. C. Zhang and R. K. Jain, "Measurements of On-Chip Waveforms and Pulse Propagation in Digital GaAs Integrated Circuits by Picosecond Electro-Optic Sampling," *Electron. Lett.* 22, 264–265 (1986).
- A. J. Taylor, R. S. Tucker, J. M. Wiesenfeld, C. A. Burrus, G. Eisenstein, J. R. Talman, and S. S. Pei, "Direct Electro-Optic Sampling of a GaAs Integrated Circuit Using a Gain-Switched InGaAsP Injection Laser," *Electron. Lett.* 22, 1068–1069 (1986).
- A. J. Taylor, J. M. Wiesenfeld, G. Eisenstein,
   R. S. Tucker, J. R. Talman, and U. Koren, "Electro-Optic Sampling of Fast Electrical Signals Using an InGaAsP Injection Laser," *Electron. Lett.* 22, 61–62 (1986).
- M. J. W. Rodwell, D. M. Bloom, and K. J. Weingarten, "Subpicosecond Laser Timing Stabilization," *IEEE J. Quantum Electron.* QE-25, 817–827 (1989).
- A. J. Taylor, J. M. Wiesenfeld, G. Eisenstein, and R. S. Tucker, "Timing Jitter in Mode-Locked and Gain-Switched InGaAsP Injection Lasers," Appl. Phys. Lett. 49, 681-683 (1986).
- J. Kluge, D. Wiechert, and D. Von der Linde, "Fluctuations in Synchronously Modelocked Dye Lasers," Opt. Commun. 51, 271–277 (1984).
- G. T. Harvey, M. S. Heutmaker, P. R. Smith, J. A. Valdmanis, and M. C. Nuss, "Timing Jitter of Colliding Pulse Modelocked (CPM) Lasers," Optical Society of America Proceedings on Picosecond Electronics and Optoelectronics, T. C. L. G. Sollner and D. M. Bloom, Eds., OSA Proceedings, Vol. 4, Optical Society of America, Washington, DC, 1989, pp. 48-51.
- J. M. Wiesenfeld, R. S. Tucker, A. Antreasyan, C. A. Burrus, A. J. Taylor, V. D. Mattera, and P. A. Garbinski, "Electro-Optic Sampling Measurements of High-Speed, InP Integrated Circuits," Appl. Phys. Lett. 50, 1310–1312 (1987).
- W. G. Spitzer and J. M. Whelan, "Infrared Absorption and Electron Effective Mass in n-Type GaAs," *Phys. Rev.* 114, 59-63 (1959)
- E. W. Van Stryland, H. Vanherzeele, M. A. Woodall, M. J. Soileau, A. L. Smirl, S. Guha, and T. F. Boggess, "Two Photon Absorption, Nonlinear Refraction, and Optical Limiting in Semiconductors," Opt. Eng. 24, 613-623 (1985).
- J. L. Freeman, D. M. Bloom, S. R. Jefferies, and B. A. Auld, "Sensitivity of Direct Electro-Optic Sampling to Adjacent Signal Lines," Appl. Phys. Lett. 54, 476-478 (1989).
- J. L. Freeman, D. M. Bloom, S. R. Jefferies, and B. A. Auld, "Accuracy of Electro-Optic Measurements of Coplanar Waveguide Transmission Lines," Appl. Phys. Lett. 53, 7-9
  (1988)
- G. A. Mourou and K. E. Meyer, "Subpicosecond Electro-Optic Sampling Using Coplanar Strip Transmission Lines," Appl. Phys. Lett. 45, 492–494 (1984).
- M. C. Nuss, P. M. Mankiewich, R. E. Howard, B. L. Straughn, T. E. Harvey, C. D. Brandle, G. W. Berkstresser, K. W. Goosen, and P. R. Smith, "Propagation of Terahertz Bandwidth Electrical Pulses on YBa<sub>2</sub>Cu<sub>3</sub>O<sub>7-8</sub> Transmission Lines on Lanthanum Aluminate," Appl. Phys. Lett. 54, 2265-2267 (1989).
- M. C. Nuss, D. W. Kisker, P. R. Smith, and T. E. Harvey, "Efficient Generation of 480 fs Electrical Pulses on Transmission Lines by Photoconductive Switching in Metalorganic Chemical Vapor Deposited CdTe," Appl. Phys. Lett. 54, 57-59 (1989).
- S. Y. Wang and D. M. Bloom, "100 GHz Bandwidth Planar GaAs Schottky Photodiode," Electron. Lett. 19, 554-555 (1983).
- R. S. Tucker, A. J. Taylor, C. A. Burrus, G. Eisenstein, and J. M. Wiesenfeld, "Coaxially Mounted 67 GHz Bandwidth InGaAs PIN Photodiode," *Electron. Lett.* 22, 917–918 (1986).
- J. E. Bowers, C. A. Burrus, and R. J. McCoy, "InGaAs PIN Photodetectors with Modulation Response to Millimeter Wavelength," *Electron. Lett.* 21, 812–814 (1985).

- 43. J. F. Jensen, K. J. Weingarten, and D. M. Bloom, "Development of 18 GHz Static Frequency Dividers and Their Evaluation by Electro-Optic Sampling," *Picosecond Electronics* and Optoelectronics II, F. J. Leonberger, C. H. Lee, F. Capasso, and H. Morkoc, Eds., Springer-Verlag, New York, 1987, pp. 184–187.
- J. F. Jensen, L. G. Salmon, D. S. Deakin, and M. J. Delaney, "Ultra-High Speed GaAs Static Frequency Dividers," *Technical Digest*, 1986 International Electron Device Meeting, pp. 476–479
- C. J. Madden, R. A. Marsland, M. J. W. Rodwell, D. M. Bloom, and Y. C. Pao, "Hyperabrupt-Doped GaAs Nonlinear Transmission Line for Picosecond Shock-Wave Generation," *Appl. Phys. Lett.* 54, 1019–1021 (1989).
- N. Suzuki and K. Tada, "Electrooptic Properties and Raman Scattering in InP," Jpn. J. Appl. Phys. 23, 291–295 (1984).
- J. A. Valdmanis and S. S. Pei, "A Non-Contact Electro-Optic Prober for High-Speed Integrated Circuits," *Picosecond Electronics and Optoelectronics II*, F. J. Leonberger, C. H. Lee, F. Capasso, and H. Morkoc, Eds., Springer-Verlag, New York, 1987, pp. 4–10.
- H. K. Heinrich, B. R. Hemenway, and D. M. Bloom, "Noninvasive Sheet Charge Density Probe for Integrated Silicon Devices," Appl. Phys. Lett. 48, 1066-1068 (1986).
- D. S. Chemla, I. Bar-Joseph, C. Klingshern, D. A. B. Miller, J. M. Kuo, and T. Y. Chang, "Optical Reading of Field-Effect Transistors by Phase-Space Absorption Quenching in a Single InGaAs Quantum Well Conducting Channel," Appl. Phys. Lett. 50, 585-587 (1987).
- U. Keller, S. K. Diamond, B. A. Auld, and D. M. Bloom, "Noninvasive Optical Probe of Free Charge and Applied Voltage in GaAs Devices," Appl. Phys. Lett. 53, 388-390 (1988).
- G. N. Koskowich and M. Soma, "Voltage Measurement in GaAs Schottky Barriers Using Optical Phase Modulation," *IEEE Electron Device Lett.* EDL-9, 433-435 (1988).
- D. S. Chemla, I. Bar-Joseph, J. M. Kuo, T. Y. Chang, C. Klingshern, G. Livescu, and D. A. B. Miller, "Modulation of Absorption in Field-Effect Quantum Well Structures," *IEEE J. Quantum Electron.* QE-24, 1664–1676 (1988).
- 53. I. Bar-Joseph, J. M. Kuo, C. Klingshern, G. Livescu, T. Y. Chang, and D. A. B. Miller, "Absorption Spectroscopy of the Continuous Transition from Low to High Electron Density in a Single Modulation-Doped InGaAs Quantum Well," *Phys. Rev. Lett.* 59, 1357-1360 (1987).
- 54. J. M. Wiesenfeld, M. S. Heutmaker, I. Bar-Joseph, D. S. Chemla, J. M. Kuo, T. Y. Chang, C. A. Burrus, and J. S. Perino, "Measurement of Multigigahertz Waveforms and Propagation Delays in Modulation-Doped Field-Effect Transistors Using Phase-Space Absorption Quenching," Appl. Phys. Lett. 55, 1109-1111 (1989).

Received July 31, 1989; accepted for publication September 22, 1989

Jay M. Wiesenfeld AT&T Bell Laboratories, Crawford Hill Laboratory, Holmdel, New Jersey 07733. Dr. Wiesenfeld received his A.B. and A.M. degrees from Harvard University in 1972, and his Ph.D. degree in chemistry from the University of California, Berkeley, in 1978. He has been at AT&T Bell Laboratories since 1978, first as a Postdoctoral Fellow and currently as a Member of Technical Staff in the Photonics Research Laboratory. Dr. Wiesenfeld's current work involves ultrashort optical pulse generation, study of components for ultra-high-speed optical communications, optical probing of electrical circuits, and study of transient behavior in optically excited materials.